On three-dimensional internal wavepackets, beams, and mean flows in a stratified fluid

by

Boyu Fan

B.S., California Institute of Technology (2015)

Submitted to the Department of Mechanical Engineering
in partial fulfillment of the requirements for the degree of

Master of Science in Mechanical Engineering

at the

MASSACHUSETTS INSTITUTE OF TECHNOLOGY

June 2017

Signature redacted

Author .....
Department of Mechanical Engineering
May 12, 2017

Signature redacted

Certified by .....
Triantaphyllos R. Akylas
Professor of Mechanical Engineering
Thesis Supervisor

Signature redacted

Accepted by .....
Rohan Abeyaratne
Chairman, Department Committee on Graduate Theses

On three-dimensional internal wavepackets, beams, and mean flows in a stratified fluid

by

Boyu Fan

Submitted to the Department of Mechanical Engineering
on May 12, 2017, in partial fulfillment of the
requirements for the degree of
Master of Science in Mechanical Engineering

Abstract

The long-time evolution and eventual dissipation mechanisms of internal waves in a stratified fluid are of fundamental geophysical importance. While much progress in recent years has been made on two-dimensional nonlinear internal wave evolution, the effects of three-dimensional variations are still poorly understood. In this thesis, we propose asymptotic models for the weakly nonlinear three-dimensional evolution of three types of internal wave disturbances: beam-like wavepackets, equally modulated wavepackets, and thin beams. Our models assess the combined effects of nonlinearity, three-dimensional modulations, viscosity, and background rotation to determine the roles that they play in wave evolution and instability.

Our results indicate that internal waves with three-dimensional variations behave in very different ways than their two-dimensional counterparts. Most notably, in all three types of waves we consider, three-dimensional variations are necessary in triggering the nonlinear transfer of energy from waves to a large-scale time-mean flow via the action of Reynolds stresses. Furthermore, we show that two distinct mechanisms of mean flow generation exist, and each may result in wave breakdown. The first is an inviscid purely modulation-induced mean flow which can trigger the so-called modulational instability. The second is a combined viscosity and modulation-driven mean flow that establishes a resonant wave–mean flow interaction known as streaming. The relative importance of these two mean flow mechanisms and associated instabilities thus depends on the specific nature of the modulations and the importance of viscous dissipation. For instance, we show that beam-like waves, where modulations are weaker in the direction along constant phase lines, exhibit the coexistence of both types of mean flow. The robust nature of the induced mean flow indicates that three-dimensional variations may be of utmost importance in determining the fate of internal waves, both in the field and in the laboratory.

Thesis Supervisor: Triantaphyllos R. Akylas
Title: Professor of Mechanical Engineering

Acknowledgments

To Professor Akylas, your wisdom, encouragement, and unsurpassed dedication have defined the researcher I am today. I've gained so much knowledge from you and I know we've barely scratched the surface.

To Professor Thomas Peacock and Professor Takeshi Kataoka, I am immensely grateful for your guidance and perspectives. Professor Peacock, thank you for welcoming me into your group as it has helped make my time at MIT a great pleasure. Professor Kataoka, thank you for your help with this work and for sharing your invaluable insights.

To the National Science Foundation Graduate Research Fellowship, DMS Grant No. 1512925, and all the people there who make this possible, your support is greatly appreciated and your work has never been more important.

To the members of the ENDLab, especially Dr. Ruth Musgrave, Rohit Supekar, Margaux Filippi, and member-in-spirit Saviz Mowlavi, thank you all for all the fantastic conversations about science and about life.

To all the new friends and all the old friends, thank you for your companionship and for being who you are. Here's to more fond memories together.

To Ann, from Pasadena to Cambridge(s), it's been quite a journey. I'm so glad to have shared it with you.

To my family, whose love and support I owe everything to, words cannot possibly do justice. I promise I'll send you more photos!

Contents

THIS PAGE INTENTIONALLY LEFT BLANK

List of Figures

Chapter 1

Introduction

Density stratified fluids support gravity waves called internal waves and their propagation and eventual dissipation are of fundamental geophysical importance. They underly the distribution of energy and momentum in the oceans and atmosphere as these dissipating waves are thought to contribute to mixing and maintaining of ocean stratification (Wunsch & Ferrari, 2004), as well as momentum transport and large scale winds (Plumb, 1977). In fact, it is estimated that as much as one terawatt of energy is dissipated by internal wave activity generated by tide–topography interactions in the deep ocean (Garrett, 2003). However, despite a great deal of progress over the recent years (see the forthcoming review by Dauxois *et al.*, 2018), there remain many open questions regarding the long time evolution of internal waves and the mechanisms by which they undergo instability. Various nonlinear mechanisms have been proposed but it remains unclear which, if any, are dominant and under what circumstances.

For example, much work thus far has focused on the triadic resonance instability for monochromatic waves, which includes the well-known parametric subharmonic instability (PSI). This class of instabilities involves resonant energy transfer to small scale subharmonic disturbances (Staquet & Sommeria, 2002; Bourget *et al.*, 2013, and others) and has been linked to oceanic mixing (MacKinnon *et al.*, 2013). However, recent work suggests that PSI may not be ubiquitous in all contexts and that there exist flow configurations that preclude PSI. Specifically, if waves are not uniformly periodic but rather locally confined, finite width effects can suppress PSI altogether (Sutherland, 2013; Bourget *et al.*, 2014; Karimi & Akylas, 2014). Therefore, this motivates the consideration of other types of instability mechanisms that may be dominant for locally confined waves.

For internal wave systems, locally confined waves hold special prominence. An

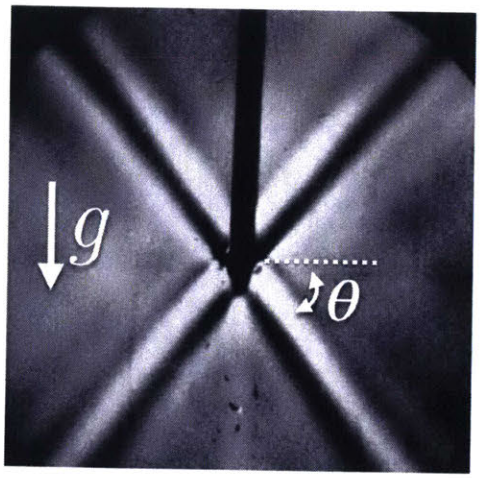

Figure 1-1: Laboratory image from Mowbray & Rarity (1967) of the four internal wave beams generated by a horizontal oscillating cylinder (coming out of the plane of the page) located at the center of the image. The four beams correspond to the four arms that radiate away from the center, forming a pattern that is known as the St. Andrew's Cross. The beam inclination angle to the horizontal, θ, is set by the frequency of oscillation of the source and given via the linear dispersion relation. The dark vertical bar is an visual artifact arising from the mechanical linkage used to oscillate the cylinder. The velocity field is nonzero only within the arms of the cross and the broadening of the beams farther from the wave source is a result of viscous dissipation.

important consequence of the natural anisotropy of a density stratified fluid is that internal waves can manifest in the form of locally confined beams, as observed in the seminal experiments by Mowbray & Rarity (1967) (see figure 1-1). Comprised of a superposition of plane waves with general wavenumber spectrum but a single temporal frequency, internal wave beams have many unique properties whose physical consequences have only recently come to light (e.g. Tabaei & Akylas, 2003). Importantly, beams are not merely theoretical or laboratory constructs. They are fundamental in geophysical contexts as they are formed readily in nature through the interaction of the tides with topography (Bell, 1975; Garrett & Kunze, 2007; Cole *et al.*, 2009; Echeverri & Peacock, 2010).

Thus far, much of the previous literature has focused on analyzing the behavior of two-dimensional internal waves. Models governing two-dimensional internal waves, with flow variations solely in a vertical plane, are simpler and computationally cheaper. However, recent experimental findings indicate that three-dimensional beams have the potential to exhibit many new types of phenomena (Bordes *et al.*, 2012; Grisouard *et al.*, 2013). Importantly, three-dimensional variations appear to catalyze an induced large-scale time-mean flow. However, much of the underlying

physics behind this three-dimensional instability mechanism is still unknown.

In this thesis, we present a theoretical study on locally confined three-dimensional internal waves. We consider various types of waves, ranging from beams to wavepackets, and show not only that three-dimensional variations are crucial in the generation of a large-scale mean flow, but also that the beam-like nature of an internal wave holds important consequences in its eventual fate.

1.1 Background

In order to provide proper context to this work, it is useful to discuss recent work on three-dimensional internal waves, followed by background on wave–mean flow interactions, which underly the evolution of three-dimensional internal waves.

1.1.1 Two-dimensional versus three-dimensional internal waves

Beginning with Mowbray & Rarity (1967), most experimental studies in the literature have focused on confined flows that are largely two-dimensional in nature. Accordingly, most of the theoretical work has followed suit in analyzing these two-dimensional flows. In these systems, a key nonlinear pathway to wave instability that has been the subject of much attention is PSI, as previously mentioned, where energy from the primary wave is transfered to subharmonic perturbations leads to dramatic breakdown of the primary wave.

The key role of three-dimensional variations in nonlinear internal wave evolution has thus gone largely unnoticed until only recently. When Bordes *et al.* (2012) experimentally forced an internal wave beam using a locally confined wave generator in a tank large enough to permit three-dimensional flow variations, they surprisingly found no PSI. Rather, they found that the internal wave beam generated a jet-like, horizontal, circulating mean flow that grew almost linearly in time. Using a preliminary analysis, they showed that a necessary condition for their observed mean flow is the presence of three-dimensional variations and dissipation. In another laboratory experiment, Grisouard *et al.* (2013) studied the reflection of an internal wave beam beam off a flat slope. They surprisingly found that the reflected beam was severely attenuated as compared to linear theory and attributed this to a large-scale mean flow that was induced in the reflection region. Using computations comparing two-dimensional with three-dimensional models, they were able to conclude that three-dimensional variations and dissipation were necessary to produce the mean flow

that they observed. Finally, it is worthwhile to note that both King *et al.* (2009) and Grisouard & Bühler (2012) had observed that internal waves generated by oscillatory three-dimensional tidal flow over topography drove a circulating horizontal mean flow in the presence of dissipation. However, as these two studies involved more complex geometries and flow-topography interactions, no direct conclusions could be drawn regarding the fundamental conditions that favor mean flow generation.

Of the work mentioned thus far, we have still not obtained a complete picture of the necessary and sufficient conditions that give rise to the wave–mean flow interaction. However, inspired by these novel results, Kataoka & Akylas (2015), hereafter referred to as KA, used a weakly nonlinear theory to model these experimental observations. By considering a thin, locally confined, modulated wave beam, KA derived fully coupled evolution equations for the wave–mean flow interaction. They were able to capture the mechanisms of mean flow generation, the feedback of the mean flow onto the waves, and confirm that indeed, three-dimensional variations are necessary. Surprisingly, they found that there were two types of mean flow generation mechanisms. One mechanism, known as streaming, relies on viscosity and is the cause of the growing mean flow. This was exactly in accordance with the conclusions drawn by Bordes *et al.* (2012) and Grisouard *et al.* (2013). The unexpected second mechanism only relied on three-dimensional modulations and not at all on dissipation. Both types of mean flow generation mechanisms, the purely modulated-induced and streaming, are each well-known in their own contexts; however, to find them coexisting in a single physical system was a novel discovery. As these two types of mean flow generation mechanisms will be crucial to the later discussion, we now aim to clarify the distinction between the two.

1.1.2 Modulation-induced mean flow

Familiar example of modulation-induced mean flows can be found in systems that are governed by nonlinear Schrödinger-like equations. The nonlinear Schrödinger equation, which describes the envelope amplitude evolution of a nearly monochromatic, weakly nonlinear and dispersive wavepacket, features a nonlinear term proportional to $|A|^2A$, where A is the slowly varying wave envelope amplitude. In general, this nonlinear term may represent both the Stokes correction to the frequency of a purely sinusoidal wave (modulations in time) as well as possible feedback of a wave-induced mean flow component. This type of nonlinear interaction relies on modulations of a periodic or uniform state and importantly, does not depend on the presence of fluid

dissipation.

As internal plane waves in a uniform stratification are exact nonlinear states, the Stokes correction to the frequency is identically zero. Thus, the nonlinear term arises solely from the feedback of an induced mean flow ($\overline{u} \propto |A|^2$), which is triggered by spatial modulations of a uniform wave. For internal wave systems, these modulation-induced mean flows can have various consequences depending on the scalings and specific system of interest. One benign possibility, occurring in the case of freely propagating internal wavepackets with three-dimensional equally strong modulations in all directions (Shrira, 1981; Bretherton, 1969; Tabaei & Akylas, 2007), is that the mean flow is simply a uniformly bounded $O(A^2)$ correction to the wave velocity field, similar to the Stokes drift of periodic deep water waves. In other systems, another more spectacular possibility is for a resonant interaction between the modulation-induced mean flow and the waves, leading to non-uniformly bounded mean flow evolution. For instance, freely propagating 'flat' wavepackets, where modulations are stronger in the vertical than horizontal direction, can couple resonantly to a modulation-induced mean flow via a 'long-wave–short-wave' interaction (Sutherland, 2001; Tabaei & Akylas, 2007). This strong interaction arises from the fact that such 'flat' modulations are compatible with low-frequency internal waves. Grimshaw (1977) also finds that a 'long-wave–short-wave' interaction is possible for modulated waves in a confined stratified channel (i.e. a constant depth ocean with rigid lids). Third and finally, it is also possible for the modulation-induced mean flow to trigger a modulational instability. As was first shown for nonlinear deep water Stokes waves (see Yuen & Lake, 1980), the modulational instability (i.e. Benjamin–Feir instability) arises from an interaction between a carrier wave and its sidebands. Specifically for internal waves, this destabilizing interaction is often mediated through the induced mean flow. For instance, 'flat' wavepackets in the weakly nonlinear limit are always modulationally unstable (Tabaei & Akylas, 2007).

1.1.3 Streaming

In contrast to modulation-induced mean flows, the second type of mean flow generation mechanism is streaming, which is most uniquely characterized by its dependence on fluid dissipation. As pointed out by Lighthill (1978), attenuated internal gravity wave beams generate a mean horizontal force that can resonantly drive a slowly varying time-mean flow. This force arises from nonuniform Reynolds stresses in a region occupied by attenuated waves. Because of the similarity of this mean flow genera-

tion mechanism with that of attenuated acoustic waves, this is known as streaming (see Riley, 2001, for a review). A typical feature of streaming is its association with vortical motions, i.e. motions that are governed by transport of vorticity or potential vorticity (PV). Specifically, McIntyre & Norton (1990) point out that it is only the irreversible transport of vorticity or PV that leads to streaming, i.e. through the action of viscous wave dissipation or wave breaking.

1.2 Motivation and outline of current work

It appears that three-dimensional effects and the resulting transfer of energy from waves to a large-scale mean flow play a much more important role in internal wave evolution than previously thought. However, the context in which this three-dimensional mean flow instability occurs remains unclear. Aside from the case of the thin beam, as discussed in KA, it remains unclear whether other systems also exhibit such behavior. Is is possible to characterize the settings in which this three-dimensional mean flow leads to wave breakdown and settings in which it does not? How do the two types of mean flow generation mechanisms come about? Does the presence of background rotation in geophysical settings affect the wave–mean interaction? These are the key questions that we will seek to address.

In Chapter 2, we study the evolution of locally confined three-dimensional modulated beam-like wavepackets. This type of internal wave disturbance is ubiquitous in laboratory settings and is a convenient and simple model to obtain theoretical insights into three-dimensional wave evolution. In § 2.1-2.3, we use a weakly nonlinear asymptotic model to predict the coupled evolution of these wavepackets and their induced mean flows. We discuss the effects of background rotation in § 2.4 and we then use this model to study their stability in § 2.5. By comparing against a recent experiment, we show in § 2.6 that our results can be used to predict physical phenomena and are not solely of theoretical merit. Overall, we find that the coexistence of the purely modulation-induced mean flow and streaming is central to the evolution of beam-like disturbances. Thus, this three-dimensional wave–mean flow interaction may be relevant for both geophysical and laboratory internal waves. In Chapter 3, we clarify and elaborate on the peculiar features that distinguish beam-like disturbances from non-beam-like disturbances. In § 3.1, we consider wavepackets that are equally modulated rather than beam-like. In § 3.2, we revisit the thin beam model of KA and examine the added effects of background rotation. Finally, Chapter 4 summarizes the major findings of this thesis.

Chapter 2

Three-dimensional beam-like internal wavepackets

As a result of modern interest in internal waves and the many unanswered fundamental questions regarding their evolution and eventual fate, laboratory experiments have played a crucial role in our current understanding. Classically, a simple method of generating beams in the laboratory is to oscillate a fixed body, such as a long cylinder, to produce four beams that emanate from the body forming a cross-like structure known as St. Andrew's Cross (Mowbray & Rarity, 1967). In this case, the thin beams generated have general profile, usually with no more than two crests (see Clark & Sutherland, 2010, for a more recent experimental study). However, with this method, it is difficult to control the wave profile and waves radiate in four directions rather than just one, introducing complications from reflections, intersections, etc. In the past decade, new methods of wave generation have overcome these setbacks by instead using a stack of offset oscillating plates (figure 2-1a) that allow precise control over the wave profile and direction (see Gostiaux *et al.*, 2007; Mercier *et al.*, 2010, and references therein). This development has allowed for the study of beams with nearly monochromatic profile in order to analyze wave instability in a controlled manner (Bordes *et al.*, 2012; Bourget *et al.*, 2013; Grisouard *et al.*, 2013; Maurer *et al.*, 2016). To our knowledge, all experiments performed in the literature to study three-dimensional internal wave beams have used nearly monochromatic profiles (e.g. figure 2-1b taken from Bordes *et al.* 2012). Therefore, we focus our attention on theoretically modeling weakly nonlinear beams with locally confined nearly monochromatic profile, hereafter referred to as wavepacket-beams. Not only are these types of waves physically relevant, they also allow us to bridge the gap between idealized sinusoidal disturbances and thin beams with general profile.

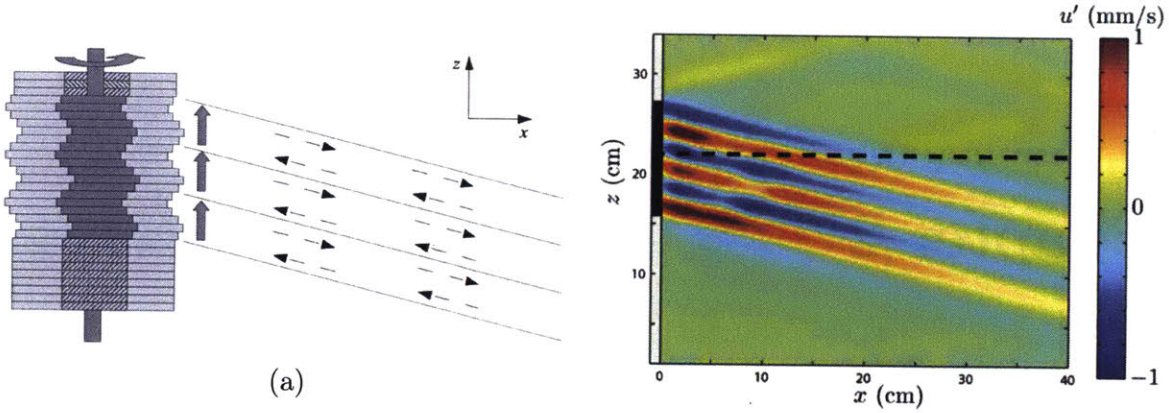

(a) (b)

Figure 2-1: (a) Schematic of a modern wave generator reproduced from Mercier *et al.* (2010), showing the oscillating stacked plates on the left, and the generated wave beam propagating to the right and downwards. Dashed arrows indicate the velocity field. (b) Experimentally obtained horizontal velocity field of an internal wave beam reported from Bordes *et al.* (2012) that was generated using a similar setup as is depicted in (a). Gravity is in the negative z-direction and the black bar on the left corresponds to the vertical extent of the wave generator. The beam emanates from the wave generator and propagates to the right. Viscosity attenuates the beam, as can be seen from the decrease in wave amplitude as it propagates. Here, the locally confined nearly monochromatic profile (with three carrier wavelengths) of the wave beam is evident.

We are interested in the propagation of internal waves in a stratified liquid such as Earth's oceans and so we make the standard Boussinesq approximation of the Navier-Stokes equations (Lighthill, 1978; Sutherland, 2010) as density variations in the ocean arising from temperature, salinity, and pressure variations only amount to a few percent. For a density stratified fluid, waves are supported through the bulk as a result of buoyancy and gravitational restoring forces. Given the background equilibrium density stratification $\overline{\rho}(y)$, where y is the vertical coordinate pointing antiparallel to gravity, the angular frequency at which a vertically displaced parcel of fluid oscillates about its equilibrium position is known as the Brunt–Väisälä frequency or buoyancy frequency and denoted N, where

$$N^2(y) = -\frac{g}{\overline{\rho}}\frac{\mathrm{d}\overline{\rho}}{\mathrm{d}y} \tag{2.1}$$

for a Boussinesq fluid. In the oceans, typical values of N range between 10^{-2} s^{-1} in the strongly stratified upper ocean (thermocline) to 10^{-4} s^{-1} in the weakly and smoothly stratified abyss (Talley, 2011), which lies roughly between 1000 km below

the surface to the ocean floor and is where much internal wave generation occurs through interactions of the tide with topography (Garrett, 2003). In this thesis, we focus on waves that propagate with vertical length scales much smaller than the length scales on which the buoyancy frequency varies. Thus, we assume a constant buoyancy frequency, in alignment with most laboratory experiments.

As the presence of Coriolis forces modifies the dispersion relation of internal waves and thus the rate of energy propagation, background rotation is an important consideration for wave evolution and stability. For example, in the case of PSI, background rotation can reinforce the ability of subharmonic perturbations to destabilize wavepackets, especially close to the critical latitude (Karimi, 2015). In the case of the wave–mean flow interaction, the effects of rotation are currently unknown. Thus, we seek to include it in our model. To do so, we make the traditional f-plane assumption by taking background rotation to be constant everywhere. Because f, the Coriolis parameter equal to twice the local background rotation rate, varies monotonically between zero at the equator to 10^{-4} s^{-1} at the poles as a result of Earth's curvature, the ratio f/N can lie anywhere between zero to values greater than one. As is well-known, internal waves are evanescent in regions where $f/N > 1$ and may only propagate in regions where $f/N < 1$. To be as general as possible, we consider the case of $f/N = O(1) < 1$ to account for strong Coriolis forces. We also discuss the results of weak rotation ($f/N \ll 1$) and no rotation ($f = 0$).

It is important to note that we ignore the possibility of PSI in this study. From a purely theoretical perceptive, monochromatic and nearly monochromatic disturbances are highly susceptible to PSI, which include wavepacket-beams and the associated scalings used in this thesis. However, laboratory experiments (e.g. Bordes *et al.*, 2012) have sometimes reported the surprising lack of PSI for beams of nearly monochromatic nature, which suggest that PSI may not always occur. Based on results in the literature, it is known that finite width effects arising from the locally confined profile of the beams can suppress PSI. To be more quantitative, Karimi & Akylas (2014) give a criterion (equation 5.14) regarding the minimum number of carrier wavelengths required for PSI to develop in a weakly nonlinear nearly monochromatic beam that is a function of beam inclination and amplitude, among other factors. For the experimental values of Bordes *et al.* (2012), whose beams only contained three carrier wavelengths, the minimum number predicted by Karimi & Akylas (2014) is 6.2. This then confirms the lack of PSI that was observed. Therefore, based on these observations and theory, we conclude that it is permissible (and still physically relevant) to ignore PSI in this study.

2.1 Governing equations and preliminaries

We consider an incompressible and unbounded uniformly stratified Boussinesq fluid rotating at a constant rate about the vertical (y-) axis. To work in nondimensional variables, we employ $1/N$ as a characteristic time scale, where N is the constant buoyancy frequency, and L as a characteristic length scale, here taken to be the carrier wavelength. In terms of the velocity field $\boldsymbol{u}$ and the excess density and excess pressure fields, ρ and p respectively, from a hydrostatic background, the nondimensional governing equations are given by

$$\boldsymbol{\nabla} \cdot \boldsymbol{u} = 0 \tag{2.2a}$$

$$\frac{\mathrm{D}\rho}{\mathrm{D}t} - \boldsymbol{u} \cdot \boldsymbol{j} = 0 \tag{2.2b}$$

$$\frac{\mathrm{D}\boldsymbol{u}}{\mathrm{D}t} + \boldsymbol{f} \times \boldsymbol{u} = -\boldsymbol{\nabla} p - \rho \boldsymbol{j} + \nu \nabla^2 \boldsymbol{u} + \boldsymbol{F}. \tag{2.2c}$$

Here, $\mathrm{D}/\mathrm{D}t \equiv \partial/\partial t + \boldsymbol{u} \cdot \boldsymbol{\nabla}$ is the material derivative, $\boldsymbol{j}$ is a unit vector pointing antiparallel to gravity, $\boldsymbol{f} = f\boldsymbol{j}$ is the constant Coriolis frequency equal to twice the background rotation rate, $\boldsymbol{F}$ is an applied force, and ν is the inverse Reynolds number given by $\nu \equiv \mu/\rho_0 N L^2$, where μ is the viscosity and ρ_0 a characteristic density.

The dispersion relation of plane internal gravity waves in the inviscid limit is given by

$$\omega^2 = \sin^2\theta + f^2 \cos^2\theta, \tag{2.3}$$

where ω is the wave frequency scaled by N and θ is the inclination angle of the wavevector to the vertical. We note that this reduces to the dispersion relation for a non-rotating system by taking $f \to 0$ and f appears as a lower cutoff frequency for propagating waves. We first consider the case of strong rotation where $f = O(1)$. Remarks will be later made for the case of weak and no rotation.

From the dispersion relation, the unique anisotropy of these systems is readily apparent, as the wave frequency depends only on the inclination angle of the wavevector, and not on its magnitude. Additionally, sinusoidal plane waves are exact nonlinear solutions of the primitive equations. As a result, a more general class of exact nonlinear solutions may be constructed via a superposition of plane waves, provided that all wavevectors are aligned in the same direction (and thus all individual components have a constant ω and θ) (Tabaei & Akylas, 2003). As previously remarked, this general class of exact nonlinear solutions are called uniform beams. To be more precise, we will work in a rotated coordinate system (ξ, η, z) with the η-direction inclined at

an angle θ with the vertical and z-direction aligned with the horizontal. Therefore, the uniform beam solution, with $\boldsymbol{u} = (u, v, w)$ along (ξ, η, z), can be expressed as

$$(u, v, w) = \left(1, 0, \frac{\mathrm{i}f\cos\theta}{\omega}\right) U(\eta) e^{-\mathrm{i}\omega t} + \text{c.c.}, \tag{2.4a}$$

$$\rho = -\frac{\mathrm{i}\sin\theta}{\omega} U(\eta) e^{-\mathrm{i}\omega t} + \text{c.c.}, \tag{2.4b}$$

$$p = \frac{\mathrm{i}(1-f^2)}{\omega} \sin\theta\cos\theta \int^{\eta} U \, \mathrm{d}\eta' \, e^{-\mathrm{i}\omega t} + \text{c.c.}, \tag{2.4c}$$

where $U(\eta)$ is a general wave profile. We will refer to these (ξ, η, z) coordinates as the along-beam, cross-beam, and transverse directions, respectively. From (2.4), it follows that the uniform wavepacket-beam can be expressed by taking,

$$U(\eta) = A(\eta) e^{\mathrm{i}l\eta}, \tag{2.5}$$

where A is a slowly varying function of η that describes the envelope and l is the carrier wavenumber. At this point, it is possible to clarify what is meant by a *beam-like disturbance*. As is evident from (2.4), uniform beams are uniform in the along-beam direction (independent of ξ). Therefore, in our consideration of modulated waves, we will consider a wave disturbance 'beam-like' if modulations in the along-beam are weaker than modulations in the across-beam direction (see Figure 2-2). This thus distinguishes beam-like disturbances from other types of disturbances, such as the equally modulated wavepacket, where modulations are equally strong in all directions, and flat wavepackets, where modulations in the horizontal are weaker than the vertical.

Just as vorticity plays a key role in the evolution of many classes of non-stratified non-rotating flows, the potential vorticity (PV) is the analogous quantity in stratified and/or rotating flows and is obtained by projecting the vorticity onto the gradient of a relevant thermodynamic tracer, ψ. In doing so, the transport of PV becomes the sole prognostic for a wide class of vortical motions that are linearly decoupled from gravity waves which carry no PV (Müller, 1995). For incompressible uniformly stratified Boussinesq fluid, the relevant fluid tracer is simply the density field. As can readily be derived from (2.2) the PV, denoted q, satisfies the evolution equation,

$$\frac{\mathrm{D}q}{\mathrm{D}t} = \boldsymbol{\nabla} \cdot \left[\nu \nabla^2 \boldsymbol{u} \times (\boldsymbol{j} - \boldsymbol{\nabla}\rho)\right], \tag{2.6}$$

where

$$q \equiv (\boldsymbol{\nabla} \times \boldsymbol{u} + \boldsymbol{f}) \cdot (\boldsymbol{j} - \boldsymbol{\nabla}\rho). \tag{2.7}$$

First, we note from (2.7) that in the linear limit, q reduces to the vertical vorticity. While q includes a constant term, f, as a result of background rotation, this constant plays no role in dynamics and is called the planetary PV. Second, in the absence of viscosity, q is a materially conserved quantity. With viscosity, this is no longer true. However, we may instead write (2.6) in integral form via the divergence theorem and show that q remains a globally conserved quantity. Third and most importantly, as can readily verified using (2.4), nonlinear plane internal gravity waves carry no PV other than the planetary PV. On the other hand, many slowly evolving (non-wave-like) large-scale vortical motions (e.g. geostrophic or quasi-geostrophic) are entirely governed by PV evolution (Müller, 1995). These flows (which exclude fast motions such as gravity waves) are characterized as being approximately 'balanced' flows (McIntyre & Norton, 1990), as the entire flow field can be uniquely determined simply by inverting the PV. As we will later show, the induced mean flow generated by modulated internal wave beams exactly corresponds to these vortical motions.

To summarize, in the linear limit, propagating waves and vortical motions (mean flows) that carry PV represent two normal modes that are entirely decoupled. In the presence of nonlinearities, where in general, modes may be coupled, uniform beams are *still* decoupled from vortical modes due to their peculiar nature as exact nonlinear solutions. It is only through the addition of *modulations* to a uniform beam that nonlinearity acts to couple waves with vortical modes. As an example to emphasize this crucial role of modulations for internal wave dynamics, it is worthwhile to note that Lelong & Riley (1991) previously analyzed the interaction between uniform sinusoidal waves (with discrete wavenumbers) and vortical modes. However, as they do not consider modulated waves (with a narrow-band spectrum), they reach the lackluster conclusion that the vortical mode does not participate in energy exchange with the waves!

2.2 Scalings

To study the evolution of a modulated wavepacket-beam, we first make a key assumption that modulations in the transverse (z-) direction vary over a length scale much larger than L. Thus, we employ a stretched coordinate,

$$Z = \varepsilon z, \quad 0 < \varepsilon \ll 1, \tag{2.8}$$

to describe these transverse variations. We assume, without loss of generality, that the applied forcing lies in the (ξ, η) plane. Accordingly, the forcing $\boldsymbol{F} = (F, H)$ in (ξ, η) is assumed to depend on the stretched coordinate, Z, and be locally confined in the ξ- and η-directions as to act as a model for a wave source. Specifically, we express F and H as

$$F = \alpha\Big\{\hat{F}(\xi, \eta, Z)e^{-\mathrm{i}\omega_0 t} + \text{c.c.}\Big\}, \quad H = \alpha\Big\{\hat{H}(\xi, \eta, Z)e^{-\mathrm{i}\omega_0 t} + \text{c.c.}\Big\}, \tag{2.9}$$

where $\hat{F}$ and $\hat{H}$ are $O(1)$ and α is a small ($\alpha \ll 1$) parameter controlling the amplitude of forcing that will later be related to ε. The forcing frequency, ω_0, thus specifies the angle of inclination, θ, of the wave beam.

We now focus our attention onto the far-field ($\xi, t \gg 1$) evolution of a wavepacket-beam driven by a time-harmonic line force with nearly monochromatic profile and weak transverse variations (2.9). Accordingly, we assume an $O(1)$ carrier wavenumber, l, in the η-direction and a slowly varying envelope. We will also allow for weak variations in the along-beam direction, and we seek a theory in the *distinguished limit* where the effects of dispersion in the transverse and along-beam directions, nonlinearity, and viscosity formally have equal weight and operate on the same slow time scale. In order to deduce the appropriate scalings for this distinguished limit, we assume that $(k_X, k_Y, k_Z) \ll l$ are characteristic wavenumbers corresponding to the modulations in (ξ, η, z), respectively. Expanding (2.3), we obtain that the modulated wave frequency can be approximated as

$$\omega^2 \sim \omega_0^2 + 2(1-f^2)\sin\theta\cos\theta\frac{k_X}{l} + (1-f^2)\cos^2\theta\frac{k_Z^2}{l^2} - 2(1-f^2)\sin\theta\cos\theta\frac{k_X k_Y}{l^2} - \omega_0^2\frac{k_X^2}{l^2} + \ldots, \tag{2.10}$$

where $\omega_0^2 \equiv \sin^2\theta + f^2\cos^2\theta$. Thus, to balance dispersive effects in the along-beam and transverse, we take the scale of along-beam modulations to be $O(\varepsilon^{-2})$. It then follows that the time scale over which these weak dispersive effects act is $O(\varepsilon^{-2})$. Accordingly, we employ the stretched coordinates

$$X = \varepsilon^2\xi, \quad T = \varepsilon^2 t, \tag{2.11}$$

to describe these modulations. For viscous dissipation to act over an $O(\varepsilon^{-2})$ length scale, we scale the viscosity

$$\nu = \beta\varepsilon^2, \tag{2.12}$$

following Lighthill (1978). While the viscosity is in essence a free parameter that we may control, we will show that the most interesting physics occurs on this scale. We will later remark on the effects of weaker or stronger viscosity. As an aside, it is important to note that other modulation scalings are indeed possible. We examine in Chapter 3 some of these other cases and we will see that behavior may qualitatively change.

For internal wave beams, (2.10) suggests that linear dispersive effects as a result of the modulations in η are a higher order effect relative to dispersion in ξ and z. Therefore, based on the scalings we have chosen thus far for the other coordinates, the scale of η-modulations (i.e. the width of the envelope) will only affect the nonlinear beam–mean flow coupling and not the linear evolution of the beam. In order to set this scale and proceed with the analysis, we note that in KA, a thin beam of $O(1)$ width, under the same modulations as discussed, induces a mean flow that extends over an $O(\varepsilon^{-1})$ width in the cross-beam direction. Thus, we choose the envelope to vary with the stretched coordinate

$$Y = \varepsilon\eta, \tag{2.13}$$

implying that modulations in the cross-beam are comparable to transverse modulations.

Finally, all that remains is to link the forcing amplitude, α, to the modulation scale, ε, such that nonlinear effects (i.e. the evolution of the mean flow) balances with dispersive effects when $T = O(1)$. From (2.4), we expect the scalings of the modulated beam flow field to be similar to that of an $O(\alpha)$ uniform beam flow field, namely

$$(u, w, \rho, p) = O(\alpha), \quad v = O(\alpha\varepsilon), \tag{2.14}$$

where the scaling for v follows from the incompressibility condition (2.2a). As it turns out, the appropriate forcing amplitude for the desired balance between weak nonlinearity and dispersion is

$$\alpha = \varepsilon. \tag{2.15}$$

Under these scalings, the appropriate expansions for our flow fields into primary

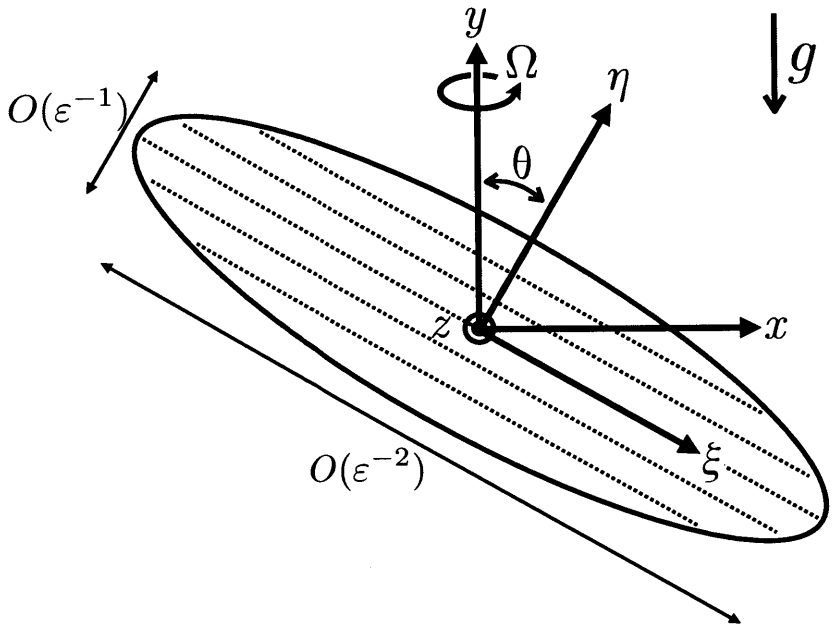

Figure 2-2: Schematic of an internal wavepacket-beam, indicating the coordinate system (ξ, η, z) corresponding to the along-beam, cross-beam, and transverse directions, respectively, the constant rotation rate about the vertical, $\Omega = f/2$, and the beam inclination angle, θ, given by the forcing frequency, ω_0. Dotted lines correspond to the constant phase lines of the sinusoidal carrier, while the bounding solid line corresponds to the finite extent of the slowly varying envelope.

harmonic and mean components are

$$u = \varepsilon\{Ue^{i\phi} + \text{c.c.}\} + \varepsilon^2\overline{U} + \ldots, \tag{2.16a}$$

$$v = \varepsilon^2\{Ve^{i\phi} + \text{c.c.}\} + \varepsilon^2\overline{V} + \ldots, \tag{2.16b}$$

$$w = \varepsilon\{We^{i\phi} + \text{c.c.}\} + \varepsilon^2\overline{W} + \ldots, \tag{2.16c}$$

$$\rho = \varepsilon\{Re^{i\phi} + \text{c.c.}\} + \varepsilon^2\overline{R} + \ldots, \tag{2.16d}$$

$$p = \varepsilon\{Pe^{i\phi} + \text{c.c.}\} + \varepsilon\overline{P} + \ldots, \tag{2.16e}$$

where $\phi \equiv l\eta - \omega_0 t$ and all primary harmonic and mean flow amplitudes (U, $\overline{U}$, etc.) are $O(1)$ functions of (X, Y, Z, T). Finally, in the far field, the forcing components $\hat{F}$ and $\hat{H}$ are approximated as

$$\hat{F} \to 2\varepsilon^2\delta(X)\{f(Y,Z)e^{il\eta} + \text{c.c.}\}, \quad \hat{H} \to 2\varepsilon^2\delta(X)\{h(Y,Z)e^{il\eta} + \text{c.c.}\}, \tag{2.17}$$

where we assume f and g are locally confined in Y. As a result, we expect the generated disturbance to vanish far from the region of forcing, i.e. as $Y \to \pm\infty$.

One might expect that in addition to a mean flow, higher order harmonics (e.g. $\propto$

$e^{-2i\omega_0 t}$, etc.) may also be generated via nonlinear interactions. However, it can be shown that the effect of the mean flow dominates over effects of higher order harmonics on the primary wave. Although we do not explicitly show this here, details are given in Kataoka & Akylas (2013) and Kataoka & Akylas (2015) for the case of the thin beam, and similar reasoning follows for our wavepacket-beam. We note that experimental observations (e.g. Bordes *et al.*, 2012; Grisouard *et al.*, 2013) have also confirmed that the mean dominates over higher harmonics for these three-dimensional internal waves.

2.3 Derivation of wave–mean evolution equations

Inserting these scalings and expansions (2.16) into the governing equations (2.2), we group terms and begin by considering those that contribute to the primary harmonic ($\propto e^{-i\omega_0 t}$). We may first obtain expressions that diagnostically relate all flow fields to the along-beam wave amplitude U. Directly from (2.2a), (2.2b), and the η- and z-components of (2.2c), we obtain to leading order,

$$V = -\frac{f\cos\theta}{\omega l}U_Z, \tag{2.18a}$$

$$W = \frac{\mathrm{i}f\cos\theta}{\omega}U, \tag{2.18b}$$

$$R = -\frac{\mathrm{i}\sin\theta}{\omega}U, \tag{2.18c}$$

$$P = \frac{1-f^2}{\omega l}\sin\theta\cos\theta\, U, \tag{2.18d}$$

where next order corrections are $O(\varepsilon)$. We note that the form of these diagnostic relations exactly corresponds to the uniform wavepacket beam solution (2.4).

With a little algebra and making use of (2.18) in the ξ-momentum equation (2.2c), we obtain at leading order an evolution equation for U given by

$$\boxed{U_T + il\overline{V}U + \frac{1-f^2}{\omega_0 l}\sin\theta\cos\theta\left[U_X - \mathrm{i}\frac{\cot\theta}{2l}U_{ZZ}\right] + \frac{\beta_E l^2}{2}U = \delta(X)f.} \tag{2.19}$$

Here,

$$\beta_E \equiv \beta\left(1 + \frac{f^2\cos^2\theta}{\omega_0^2}\right) \tag{2.20}$$

is an effective viscosity due to added dissipative effects from background rotation. We will see that this effective viscosity persists throughout this thesis as one of the effects

of $O(1)$ background rotation. In assessing the physics of this evolution equation, we first confirm that our scalings result in a leading order balance between nonlinearity, dispersion, and viscosity. Going term by term from the left, the second term corresponds to the nonlinear feedback of the wave-induced mean flow onto the waves, which is felt through the action of the cross-beam mean flow component, $\overline{V}$, that is as of yet undetermined. The third term arises from along-beam modulations and results in propagation at a velocity given by the group velocity. The fourth term arises from transverse modulations and results in Schrödinger-like dispersion. The fifth and final term on the left hand side corresponds to the effect of viscous dissipation that thus far simply results in an exponential decay in the wave amplitude. We note that as expected for modulated beams, the waves are not linearly affected by cross-beam modulations as (2.19) has no Y-dependence.

Turning to the mean flow terms, we obtain directly from (2.2) diagnostic equations that relate all mean flow fields to $\overline{V}$:

$$\overline{U} = \cot\theta\,\overline{V}, \tag{2.21a}$$

$$\overline{W}_Z = -\overline{V}_Y, \tag{2.21b}$$

$$\overline{R}_Z = -f\cot\theta\,\overline{V}_Y, \tag{2.21c}$$

$$\overline{P}_Z = f\csc\theta\,\overline{V}, \tag{2.21d}$$

where all next order corrections are $O(\varepsilon)$. We immediately see from (2.21a) that the mean flow is purely horizontal to leading order. All that remains now is to find an evolution equation for $\overline{V}$ to obtain a closed system with (2.19). While it is possible to proceed, with considerable algebra, directly from (2.2), we instead appeal to PV evolution (2.6) and (2.7) as we anticipate that the mean flow response is governed by the mean PV.

Making use of our scalings and expansions, q can be expressed in terms of its primary harmonic and mean components as

$$q = f + \varepsilon^3\left\{Qe^{\mathrm{i}(l\eta-\omega_0 t)} + \text{c.c.}\right\} + \varepsilon^3\overline{Q} + \ldots, \tag{2.22}$$

where the $O(1)$ amplitudes Q and $\overline{Q}$ are functions of (X, Y, Z, T). The first term on the right hand side, representing the constant planetary vorticity, has been explicitly separated from $\overline{Q}$ since as a constant, it plays no further role in PV evolution. From

(2.6), we find that the primary harmonic is diagnostically given by

$$Q = -\beta \frac{il^3 f \sin\theta \cos\theta}{\omega_0^2} U + O(\varepsilon), \tag{2.23}$$

while the mean PV evolves according to

$$\overline{Q}_T = \frac{2\beta l^3 \sin\theta}{\omega_0}\left(1 + \frac{f^2 \cos^2\theta}{\omega_0^2}\right)(U^* U)_Z + O(\varepsilon). \tag{2.24}$$

This brings out the role of nonlinearity, three-dimensional variations, and viscosity in the production of mean PV. Finally, it remains to relate $\overline{Q}$ to the mean flow field to obtain a closed set of evolution equations with (2.19). To do so, we make use of (2.7) to express $\overline{Q}$ in terms of the flow velocities,

$$\overline{Q} = \frac{1}{\sin\theta}\left(\overline{V}_Z - \omega_0^2 \overline{W}_Y\right) - \frac{2l \sin\theta}{\omega_0}(U^* U)_Z + O(\varepsilon). \tag{2.25}$$

Combining (2.25) with (2.24) and (2.21), it follows that the evolution of $\overline{V}$ can be written as

$$\boxed{\frac{\partial}{\partial T}\left[\overline{V}_{ZZ} + \omega_0^2 \overline{V}_{YY} - \frac{2l \sin^2\theta}{\omega_0}(U^* U)_{ZZ}\right] = \frac{2\beta_E l^3 \sin^2\theta}{\omega_0}(U^* U)_{ZZ}.} \tag{2.26}$$

Together, (2.19) and (2.26) form a closed system of evolution equations for U and $\overline{V}$ describing the interaction between nonlinear three-dimensional modulated wavepacket-beams and their induced mean flows.

From the nonlinear terms in (2.26), we see that there are *two mechanisms* of mean flow production: an inviscid purely modulation-induced term appearing on the left hand side, as well as a viscous term appearing on the right hand side. First, let us consider the dynamics in the inviscid limit ($\beta \to 0$). In this case, mean flow only arises from the purely modulation-induced mechanism. The right hand side of (2.26) is zero and (2.26) can be trivially integrated in time for a given initial condition. Thus, the mean flow is governed by a Poisson equation, does not evolve separately from the waves, and remains asymptotically bounded barring any modulational instabilities. Given the wave field at any given instant in time, the mean flow can be diagnostically determined from (2.26) and in this sense, the mean flow is 'slaved' to the waves in the inviscid limit. Next, let us consider the effect of nonzero viscosity. In this case, (2.26) does not reduce to a Poisson equation as it cannot be trivially integrated. Rather, the nonlinear source term on the left hand side proportional to β triggers resonant

mean flow growth, i.e. streaming. Regardless of the presence of viscous dissipation, *transverse modulations are essential* as they produce nonuniform Reynolds stresses which result in both mechanisms of mean flow generation.

We confirm that the mean flow is a 'balanced' flow in the sense of McIntyre & Norton (1990), as it is possible to invert a given PV field and obtain the velocity field at any time via (2.23) and (2.18) for the primary harmonic and via (2.25) and (2.21) for the mean flow. According to (2.25), the modulation-induced mean flow arises from the material conservation of PV under inviscid flow conditions. Streaming arises from the irreversible production of mean PV from viscous wave attenuation, as pointed out by McIntyre & Norton (1990). While the beam equation (2.19) for wavepacket-beams resembles that of thin beams (KA, equation 3.9), the mean flow equation (2.26) is significantly different from that of the thin beam (KA, equation 4.13). Nonetheless, for the wavepacket-beam, both mean flow generation mechanisms persist and operate on the same time scale.

2.4 Effects of background rotation

Remarkably, the effect of $O(1)$ background rotation on the evolution equations is minimal, appearing only in the coefficients. One effect, as we have already noted, is an increased effective viscosity resulting from the combined action of molecular viscosity and rotation. While this increases the effective viscous dissipation acting on the beam, it also enhances streaming. In order to assess the effects of rotation on the linear dispersive terms of (2.19), we note that we may eliminate θ using the dispersion relation. Thus, (2.19) can be equivalently written as

$$U_T + il\overline{V}U + \sqrt{\left(1-\frac{f^2}{\omega_0^2}\right)\left(1-\omega_0^2\right)}U_X - \mathrm{i}\frac{1-\omega_0^2}{2\omega_0 l^2}U_{ZZ} + \frac{\beta_E l^2}{2}U = \delta(X)f. \qquad (2.27)$$

Therefore, for a fixed forcing frequency ω_0, as is the case of tidal forcing, increasing background rotation monotonically reduces the rate of propagation in the along-beam direction, i.e. the group velocity, as the beam becomes more horizontal. However, given a fixed ω_0, rotation does not affect dispersion in the z-direction. To obtain a more complete picture of the effects of rotation, we now consider the case of no rotation and weak rotation.

2.4.1 Case of no rotation

It is possible to follow a similar analysis for the evolution of a modulated wavepacket-beam with no background rotation. In this case, the linear dispersion relation is simply given by

$$\omega^2 = \sin^2\theta, \tag{2.28}$$

while the uniform beam velocity field, still an exact nonlinear state, is now given by

$$(u, v, w) = (1, 0, 0)\, U(\eta) e^{-\mathrm{i}\omega t} + \text{c.c.} \tag{2.29}$$

We now quote the end result of the analysis. As it turns out, taking $f = 0$ in (2.19) and (2.26) recovers the evolution equations in the absence of rotation, although the scalings for the various flow fields, and thus the diagnostic relations between U, $\overline{V}$, and the other flow components, do not reduce so conveniently.

To rigorously demonstrate this, we may start again from first principles assuming a modulated wavepacket-beam with $O(\varepsilon)$ modulations in z and forced with frequency $\omega_0 = \sin\theta$. Via (2.10) with $f = 0$, we see that the scales for ξ-modulations and slow time T remain unchanged as before in order to capture the leading order effects of dispersion. For nonlinearity to act on the same time scale as dispersion, such that the mean flow evolves over the slow time variable, the flow expansions in terms of primary harmonic and mean components must now be taken as,

$$u = \varepsilon\{U e^{\mathrm{i}\phi} + \text{c.c.}\} + \varepsilon^2 \overline{U} + \ldots, \tag{2.30a}$$
$$v = \varepsilon^3\{V e^{\mathrm{i}\phi} + \text{c.c.}\} + \varepsilon^2 \overline{V} + \ldots, \tag{2.30b}$$
$$w = \varepsilon^2\{W e^{\mathrm{i}\phi} + \text{c.c.}\} + \varepsilon^2 \overline{W} + \ldots, \tag{2.30c}$$
$$\rho = \varepsilon\{R e^{\mathrm{i}\phi} + \text{c.c.}\} + \varepsilon^4 \overline{R} + \ldots, \tag{2.30d}$$
$$p = \varepsilon\{P e^{\mathrm{i}\phi} + \text{c.c.}\} + \varepsilon^3 \overline{P} + \ldots, \tag{2.30e}$$

where $\phi \equiv l\eta - \sin\theta\, t$. Note that the differences from the rotating system lie in the scalings for V, W, $\overline{R}$, and $\overline{P}$, which are now all asymptotically smaller than those for the case of strong rotation. In the cross-beam direction, the mean flow component turns out to be larger than the wave component. Previously, in the case of strong rotation, an $O(\varepsilon)$ excess mean pressure was necessary to balance the Coriolis force acting on the induced mean flow, i.e. a quasi-geostrophic flow. In the absence of rotation and Coriolis forces, the excess mean pressure field, as well as the excess density field, must now be rescaled accordingly. Taking these modified scalings into

account, we may once again derive coupled evolution equations for U and $\overline{V}$ which exactly correspond to (2.19) and (2.26) for $f = 0$. All other flow fields can still be obtained diagnostically and the mean flow remains horizontal at leading order.

2.4.2 Case of weak rotation

Here, we consider the effects of weak rotation, where $f \ll 1$, and once again take the distinguished limit. For weak rotation to act on the $O(\varepsilon^2)$ time scale of weak dispersion, we see from (2.10) that we must take $f = O(\varepsilon)$. By rescaling,

$$f \to \varepsilon f, \tag{2.31}$$

and making use of (2.10), the linear dispersion relation for sinusoidal waves can thus be approximated as

$$\omega \approx \sin\theta + \varepsilon^2 \frac{f^2 \cos^2\theta}{2\sin\theta} + \ldots, \tag{2.32}$$

As it turns out, the desired balance of weak rotation, dispersion, nonlinearity, and viscosity occurs for a $O(\varepsilon)$ amplitude wavepacket-beam as before. However, it is necessary to introduce new scalings for the flow field expansions, namely,

$$u = \varepsilon\{Ue^{\mathrm{i}\phi} + \text{c.c.}\} + \varepsilon^2\overline{U} + \ldots, \tag{2.33a}$$

$$v = \varepsilon^3\{Ve^{\mathrm{i}\phi} + \text{c.c.}\} + \varepsilon^2\overline{V} + \ldots, \tag{2.33b}$$

$$w = \varepsilon^2\{We^{\mathrm{i}\phi} + \text{c.c.}\} + \varepsilon^2\overline{W} + \ldots, \tag{2.33c}$$

$$\rho = \varepsilon\{Re^{\mathrm{i}\phi} + \text{c.c.}\} + \varepsilon^3\overline{R} + \ldots, \tag{2.33d}$$

$$p = \varepsilon\{Pe^{\mathrm{i}\phi} + \text{c.c.}\} + \varepsilon^2\overline{P} + \ldots, \tag{2.33e}$$

where $\phi \equiv l\eta - \sin\theta\, t$ in view of (2.32). In the case of weak rotation, we see as expected that the scalings of the mean excess pressure and density fields lie between those for strong rotation and no rotation. Inserting these scalings into our governing equations and following a similar analysis as before, we obtain that the wave amplitude is governed by

$$U_T + il\overline{V}U + \frac{\cos\theta}{l}\left[U_X - \mathrm{i}\frac{\cot\theta}{2l}U_{ZZ}\right] + \frac{\beta l^2}{2}U + \mathrm{i}\frac{f^2\cos^2\theta}{2\sin\theta}U = \delta(X)f, \tag{2.34}$$

while the mean flow amplitude is governed by

$$\frac{\partial}{\partial T}\left[\overline{V}_{ZZ} + \sin^2\theta\,\overline{V}_{YY} - 2l\sin\theta(U^*U)_{ZZ}\right] = 2\beta l^3\sin\theta(U^*U)_{ZZ}. \tag{2.35}$$

Thus, the effect of rotation is simply a $O(\varepsilon^2)$ frequency shift that can be eliminated from the equations (2.34) and (2.35) via the substitution

$$U \to U \exp\left(-\mathrm{i}\frac{f^2 \cos^2\theta}{2\sin\theta}T\right), \tag{2.36}$$

exactly reducing them to the evolution equations in the absence of background rotation. All other flow components can be diagnostically obtained from U and $\overline{V}$ and not surprisingly, we observe that the mean flow is horizontal to leading order, as $\overline{U} = \overline{V}\cot\theta + O(\varepsilon^2)$.

To summarize, we have conduced a systematic analysis of the effects of rotation on the wave–mean flow interaction by considering strong, weak, and no rotation. Even in the case of strong rotation, we find that rotation plays a minimal role in the reduced equations, merely adjusting the coefficients. It is important to emphasize that while the coupled evolution equations (2.19) and (2.26) governing U and $\overline{V}$ are relatively insensitive to rotation, the other flow fields are affected in both scalings and form, although they may still be diagnostically obtained from U and $\overline{V}$.

2.5 Inviscid stability analysis

The wavepacket-beam–mean flow interaction equations derived above highlight the coexistence of two nonlinear mechanisms for mean flow generation, one inviscid and one viscous in nature. Whereas the effect of streaming is resonant mean flow growth, the effect of the inviscid modulation-induced mean flow is not immediately obvious. Here, based on our model, we study the effect of the inviscid mean flow and determine whether it can trigger wave instability. To do so, we examine stability of free uniform wavepacket-beams to three-dimensional perturbations in the inviscid limit ($\beta = 0$). In order to study the stability of both progressive and standing wavepacket-beams, we first generalize the results of the previous section to multiple wavepackets with varying carrier wavenumbers but constant frequency. We now also return to the case of $f = O(1)$. Because much of the analysis is similar, we simply provide the key differences and state the ensuing results.

2.5.1 Generalization to multiple wavepackets

To describe the far field evolution of multiple modulated wavepackets, we first introduce multiple $O(1)$ carrier wavenumbers l_j indexed by j, and rewrite the forcing

component $\hat{F}$ in the far field as

$$\hat{F} \to 2\varepsilon^2\delta(X)\sum_j \left\{f_j(Y,Z)e^{\mathrm{i}l_j\eta} + \text{c.c.}\right\}, \tag{2.37}$$

where f_j is the forcing amplitude of the component with carrier wavenumber l_j. As $\hat{H}$, the forcing component in the η-direction, only contributes a higher order effect, we may ignore it. Next, the primary harmonic–mean expansion, taking into account multiple wavepacket-beams, is rewritten as

$$u = \varepsilon\sum_j \left\{U_j e^{\mathrm{i}\phi_j} + \text{c.c.}\right\} + \varepsilon^2\overline{U} + \ldots, \tag{2.38a}$$

$$v = \varepsilon^2\sum_j \left\{V_j e^{\mathrm{i}\phi_j} + \text{c.c.}\right\} + \varepsilon^2\overline{V} + \ldots, \tag{2.38b}$$

$$w = \varepsilon\sum_j \left\{W_j e^{\mathrm{i}\phi_j} + \text{c.c.}\right\} + \varepsilon^2\overline{W} + \ldots, \tag{2.38c}$$

$$\rho = \varepsilon\sum_j \left\{R_j e^{\mathrm{i}\phi_j} + \text{c.c.}\right\} + \varepsilon^2\overline{R} + \ldots, \tag{2.38d}$$

$$p = \varepsilon\sum_j \left\{P_j e^{\mathrm{i}\phi_j} + \text{c.c.}\right\} + \varepsilon\overline{P} + \ldots, \tag{2.38e}$$

where $\phi_j \equiv l_j\eta - \omega_0 t$. Inserting these expansions, we obtain that each wavepacket-beam amplitude U_j evolves according to

$$U_{jT} + il_j\overline{V}U_j + \frac{1-f^2}{\omega_0 l_j}\sin\theta\cos\theta\left[U_{jX} - \mathrm{i}\frac{\cot\theta}{2l_j}U_{jZZ}\right] + \frac{\beta_E l_j^2}{2}U_j = \delta(X)f_j, \tag{2.39}$$

and mean flow $\overline{V}$ evolves according to

$$\frac{\partial}{\partial T}\left[\overline{V}_{ZZ} + \omega_0^2\overline{V}_{YY} - \frac{2\sin^2\theta}{\omega_0}\sum_j l_j\left(U_j^*U_j\right)_{ZZ}\right] = \frac{2\beta_E\sin^2\theta}{\omega_0}\sum_j l_j^3\left(U_j^*U_j\right)_{ZZ}. \tag{2.40}$$

Thus, the interaction between multiple wavepacket-beams is solely mediated through the mean flow, which includes contributions from each wavepacket-beam.

2.5.2 Derivation of eigenvalue problem

Based on these evolution equations, we may now derive the eigenvalue problem governing the stability of free uniform wavepacket-beams in the inviscid limit. First, we normalize our equations such that the dependence on θ and f is scaled out. Intro-

ducing the changes of variable,

$$U = \frac{1}{\sin\theta}\sqrt{\frac{\omega_0}{2}}\,\tilde{U}, \tag{2.41a}$$

$$X = \frac{(1-f^2)\sin\theta\cos\theta}{\omega_0}\tilde{X}, \tag{2.41b}$$

$$(Y,Z) = \cos\theta\sqrt{\frac{1-f^2}{2\omega_0}}\,(\omega_0\tilde{Y},\tilde{Z}), \tag{2.41c}$$

the coupled system in normalized form is given by

$$\tilde{U}_{jT} + il_j\overline{V}\tilde{U}_j + \frac{1}{l_j}\tilde{U}_{j\tilde{X}} - \mathrm{i}\frac{1}{l_j^2}\tilde{U}_{j\tilde{Z}\tilde{Z}} = 0, \tag{2.42a}$$

$$\overline{V}_{\tilde{Z}\tilde{Z}} + \overline{V}_{\tilde{Y}\tilde{Y}} = \sum_j l_j(\tilde{U}_j^*\tilde{U}_j)_{\tilde{Z}\tilde{Z}}, \tag{2.42b}$$

subject to boundary conditions,

$$(\tilde{U},\overline{V}) \to 0 \qquad (\tilde{Y}\to\pm\infty), \tag{2.43}$$

as we expect locally confined evolution from locally confined waves.

We wish to examine the linear stability of a base state composed of a superposition of uniform wavepacket-beams, $\tilde{U}_j = \tilde{U}_j^B(\tilde{Y})$, to infinitesimal along-beam and transverse perturbations. As our base state depends on $\tilde{Y}$ only, we superpose perturbations in the form of normal modes in $\tilde{X}$, $\tilde{Z}$, and T such that our flow field can be expanded as

$$\tilde{U}_j = \tilde{U}_j^B(\tilde{Y}) + \hat{u}_{j+}(\tilde{Y})e^{\mathrm{i}(k\tilde{X}+m\tilde{Z}-\sigma T)} + \hat{u}_{j-}^*(\tilde{Y})e^{-\mathrm{i}(k\tilde{X}+m\tilde{Z}-\sigma T)}, \tag{2.44a}$$

$$\overline{V} = \overline{v}(\tilde{Y})e^{\mathrm{i}(k\tilde{X}+m\tilde{Z}-\sigma T)} + \text{c.c.} \tag{2.44b}$$

Here, k and m are given real wavenumbers, σ is an undetermined, possibly complex frequency, and $\hat{u}_{j+}$, $\hat{u}_{j-}$, and $\overline{v}$ are undetermined mode shapes. Substituting into (2.42a) and linearizing with respect to the perturbations, it turns out that we may derive a single eigenvalue equation. First, it is possible to express $\hat{u}_{j+}$ and $\hat{u}_{j-}$ in

terms of $\overline{v}$ as follows:

$$\hat{u}_{j+} = \frac{l_j \tilde{U}_j^B}{\sigma - \frac{k}{l_j} - \frac{m^2}{l_j^2}} \overline{v}, \tag{2.45a}$$

$$\hat{u}_{j-} = -\frac{l_j \tilde{U}_j^{B*}}{\sigma - \frac{k}{l_j} + \frac{m^2}{l_j^2}} \overline{v}. \tag{2.45b}$$

Making use of (2.44) and (2.45) in (2.42b), we obtain a single eigenvalue problem for $\overline{v}(\tilde{Y})$ with eigenvalue σ as,

$$\overline{v}_{\tilde{Y}\tilde{Y}} - m^2 \overline{v} = -\left(\sum_j \frac{2m^4}{(\sigma - \frac{k}{l_j})^2 - \frac{m^4}{l_j^4}} \left| \tilde{U}_j^B \right|^2 \right) \overline{v}, \tag{2.46}$$

subject to boundary conditions

$$\overline{v} \to 0 \qquad (\tilde{Y} \to \pm\infty). \tag{2.47}$$

Therefore, given uniform wavepacket-beam profiles, $\tilde{U}_j^B(\tilde{Y})$, and associated l_j, it remains to solve for σ, where the existence of $\sigma^2 < 0$ implies instability.

2.5.3 Progressive beams

For a single progressive wavepacket-beam, our base state consists of a single uniform wavepacket-beam $\tilde{U}^B(Y)$ and wavenumber l. The eigenvalue problem thus reduces to

$$\overline{v}_{\tilde{Y}\tilde{Y}} - m^2 \overline{v} = -\frac{2m^4}{(\sigma - \frac{k}{l})^2 - \frac{m^4}{l^4}} \left| \tilde{U}^B \right|^2 \overline{v}. \tag{2.48}$$

Multiplying this equation by $\overline{v}^*$, integrating in $\tilde{Y}$ over the domain $(-\infty, \infty)$, and making use of (2.47), it follows that

$$\frac{\int_{-\infty}^{\infty} \left(|\overline{v}_{\tilde{Y}}|^2 + m^2 |\overline{v}|^2 \right) \mathrm{d}\tilde{Y}}{\int_{-\infty}^{\infty} \left| \tilde{U}^B \right|^2 |\overline{v}|^2 \, \mathrm{d}\tilde{Y}} = \frac{2m^4}{(\sigma - \frac{k}{l})^2 - \frac{m^4}{l^4}} \equiv \lambda. \tag{2.49}$$

Therefore, λ must be real and positive for any given wave profile. Solving for σ in terms of λ, we obtain

$$\sigma = \frac{k}{l} \pm m^2 \sqrt{\frac{2}{\lambda} + \frac{1}{l^4}} \tag{2.50}$$

and in light of (2.49), we conclude that σ is purely real for any given profile. Therefore, we conclude that weakly nonlinear progressive wavepacket-beams are stable to infinitesimal three-dimensional perturbations.

2.5.4 Standing beams

A standing wavepacket-beam is comprised of two progressive wavepacket-beams with carrier wavenumbers given by $l_1 = -l_2 \equiv l$ and corresponding uniform beam profiles $\tilde{U}_1^B = \tilde{U}_2^B \equiv \tilde{U}^B$. Thus, the eigenvalue problem for a standing wavepacket-beam reduces to

$$\overline{v}_{\tilde{Y}\tilde{Y}} - m^2\overline{v} = -\Lambda\left|\tilde{U}_B\right|^2\overline{v}, \tag{2.51}$$

where

$$\Lambda \equiv 2m^4\left\{\frac{1}{(\sigma - \frac{k}{l})^2 - \frac{m^4}{l^4}} + \frac{1}{(\sigma + \frac{k}{l})^2 - \frac{m^4}{l^4}}\right\}. \tag{2.52}$$

Once again, by integrating (2.51) against $\overline{v}^*$ and making use of the boundary condition (2.47), we may show that

$$\int_{-\infty}^{\infty}\left(|\overline{v}_{\tilde{Y}}|^2 + m^2|\overline{v}|^2\right)\mathrm{d}\tilde{Y} = \Lambda\int_{-\infty}^{\infty}\left|\tilde{U}^B\right|^2|\overline{v}|^2\,\mathrm{d}\tilde{Y}\,. \tag{2.53}$$

Therefore, Λ must be real and positive for any given wave profile $\tilde{U}^B$. Solving for σ in terms of Λ, it follows that if the condition

$$\frac{1}{l^2} < \frac{k^2}{m^4} < \frac{1}{l^2} + \frac{4l^2}{\Lambda} \tag{2.54}$$

is satisfied, then $\sigma^2 < 0$, implying instability. As Λ must be real and positive, then for any finite Λ, there always exists a finite window of perturbation wavenumbers k and m that result in instability. Therefore, we may conclude that the standing wavepacket-beam is unstable to three-dimensional perturbations. Importantly, both along-beam and transverse perturbation are necessary.

2.5.5 General stability remarks

Thus far, we have been able to make analytic progress in determining the stability of single progressive wavepacket-beams and standing wavepacket-beams. In general, the stability of multiple wavepacket-beams with different envelopes and carrier wavenumbers must be determined by solving the corresponding eigenvalue problem

numerically.

As the stability of progressive and standing wavepacket-beams is independent of background rotation, it is possible to compare these results against the inviscid modulational stability of thin beams as considered in Kataoka & Akylas (2013) and Kataoka & Akylas (2016). Both studies discuss, among other problems, the stability of weakly nonlinear three-dimensional thin beams of $O(1)$ cross-beam width and general profile. These thin beams were subject to the same along-beam and transverse modulations as considered here for the wavepacket-beam. We note that it was necessary to numerically solve the eigenvalue problem in the case of the thin beam, while we were able to make analytic progress here in the case of the wavepacket-beam. For both wavepacket-beams and thin beams, standing waves are unstable. Additionally, we showed that unstable eigenvalues for the standing wavepacket-beam arise only for a finite range of k/m^2, a result that resembles that for standing thin beams (Kataoka & Akylas, 2013, figure 7).

We showed in § 2.5.3 that single progressive wavepacket-beams are always stable. On the other hand, progressive thin beams, comprised of a spectrum of wavenumbers of the same sign, can be either stable or unstable depending on the specific wave profile and amplitude (Kataoka & Akylas, 2013). The difference between the behavior of the thin beam and wavepacket-beam can be rationalized in two ways. First, the weakly nonlinear analysis of the wavepacket-beam in the distinguished limit requires a beam amplitude of $O(\varepsilon)$, while the thin beam analysis requires a higher amplitude, $O(\varepsilon^{1/2})$. Therefore, it is possible that differing wave amplitudes results in the differing stability properties of thin beams and wavepacket-beams. Second, the wavenumber spectrum of progressive wavepacket-beams is sharply peaked about a single carrier wavenumber, whereas the thin beam features a general spectrum of wavenumbers. Although we do not rigorously prove this here, it appears that base states consisting of two or more progressive wavepacket-beams with varying carrier frequencies are typically unstable. As a special case, when two progressive waves have the same envelope with carrier frequencies $l_1 = -l_2$, i.e. the standing beam, instability is guaranteed.

2.6 Comparison with Bordes *et al.* (2012)

We now directly compare our wavepacket-beam model (without background rotation) with the laboratory experiment by Bordes *et al.* (2012). Previously, the results of the same laboratory experiment was utilized by KA as a validation of their three-dimensional thin beam model. However, while the thin beam model was successful

in predicting the overall qualitative nature of the jet-like mean flow, amongst other features, it was less successful in reaching quantitative agreement. Largely, this was because the scaling assumptions for a thin beam were poorly met by the experimental parameters. Specifically, the wave generator of Bordes *et al.* (2012) had nearly monochromatic profile, with carrier wavelength $L = 3.8$ cm, fixed vertical height $3L$, and transverse width $3.7L$. Given the ratio of vertical to lateral extent of the forcing is about 0.8, the experimental setup much better satisfies the scalings of our wavepacket-beam analysis, as the transverse length scale is on the order of the cross-beam envelope width.

First, we nondimensionalize the experimental parameters of Bordes *et al.* (2012), where $N = 0.85$ s^{-1} and $L = 3.8$ cm are the (inverse) time scale and length scale, respectively, and $\omega_0 = 0.26$. We select ε so that the transverse width of the wave generator is normalized to unity (in terms of Z). Using (2.8) and (2.12), this specifies $\varepsilon = 0.27$ and $\beta \doteq 0.011$. The evolution equations (2.19) and (2.26) for $f = 0$ are solved numerically from an initially quiescent fluid at $T = 0$ using pseudo-spectral discretization in $Y \in [-4, 4]$ and $Z \in [-4, 4]$ using 256×128 Fourier modes, a third-order upwind finite difference scheme in $X \in [0, 1]$ with $\Delta X = 0.001$, and fourth-order Runge–Kutta time marching with $\Delta T = 0.008$. In our numerical implementation, rather than employing the forcing function $f(Y, Z)$ in the momentum equations, we instead enforced a boundary condition specifying the wave profile at $X = 0$ in order to mimic the action of the wavemaker. With $l = 2\pi$, we approximate the rectangular wavemaker by using the boundary (wavemaker) profile

$$U(X=0) = A_0\Big\{\tanh\big[5(Z+0.5)\big] - \tanh\big[5(Z-0.5)\big]\Big\}\Big\{\tanh\big[15(Y+0.41)\big] - \tanh\big[15(Y-0.41)\big]\Big\}, \quad (2.55)$$

where $A_0 = 0.06$ so that the maximum wave x-velocity matches the maximum experimental value of 1 mm s^{-1}. It is worthwhile to note that the wavepacket-beam evolution equations are computationally much less expensive than the thin beam evolution equations of KA.

In figure 2-3, we show the experimental results from Bordes *et al.* (2012) which plot the observed x-velocity of the wave field and mean flow field. In figure 2-4, we show the exactly analogous plots of the wave and mean flow fields as predicted by our evolution equations. We see excellent agreement between the observed and predicted flow fields. For the same flow system, it is also now possible to compare our results with the theoretical predictions made by KA using a thin beam model (see figure 2 in

KA) rather than a wavepacket-beam model. While the evolution of the wave beam is largely unchanged between the two theories, the mean flow in the wavepacket-beam model agrees much better with the experimental observations than that from the thin beam model. Most noticeably, the wavepacket-beam generates a mean flow that extends farther from the wavemaker, rather than the strongly localized mean flow generated by the thin mean. Furthermore, the wavepacket-beam equations predict that the mean flow grows at a slower rate, reaching comparable amplitudes to the experiment at $t = 323$ s rather than $t = 96$ s for the thin beam. Note that Bordes *et al.* (2012) do not the report the time after the wavemaker is turned on at which their data was collected.

2.7 Summary and conclusions

We have proposed a model that describes the evolution of three-dimensionally modulated beam-like wavepackets, where modulations are weaker in the along-beam direction, i.e. along lines of constant phase. Our model incorporates the combined effects of weak nonlinearity, dispersion, viscosity, and background rotation and our fully coupled evolution equations, (2.19) and (2.26), capture both the evolution of the wave-induced mean flow as well as the feedback of the mean flow on the waves.

Our model has revealed a great deal of physics regarding the evolution and eventual fate of internal wave beams. First and foremost, three-dimensional variations trigger behavior that is entirely different from two-dimensional systems, i.e. the generation of a large-scale time mean flow. More specifically, there are two unique mechanisms of mean flow generation, one inviscid and purely-modulation induced and another relying on viscous dissipation (streaming). Both mechanisms can lead to dramatic beam breakdown, the former via modulational instability (§ 2.5) and the latter via resonant mean flow growth. Both mechanisms coexist, suggesting that our model is relevant to both laboratory settings, where viscosity is unavoidably important, and geophysical settings, where viscosity is relatively less important and modulational instability must be taken into consideration.

In the presence of background rotation, the mean PV emerges as the signature of the mean flow, which corresponds to a purely horizontal zero-frequency mode of motion. The mean PV thus generalizes the role of vertical vorticity in non-rotating systems. However, we have shown that background rotation does not significantly affect the dynamics of the wave–mean interaction. Therefore, the results we have presented here can be generally applied to both laboratory and geophysical settings.

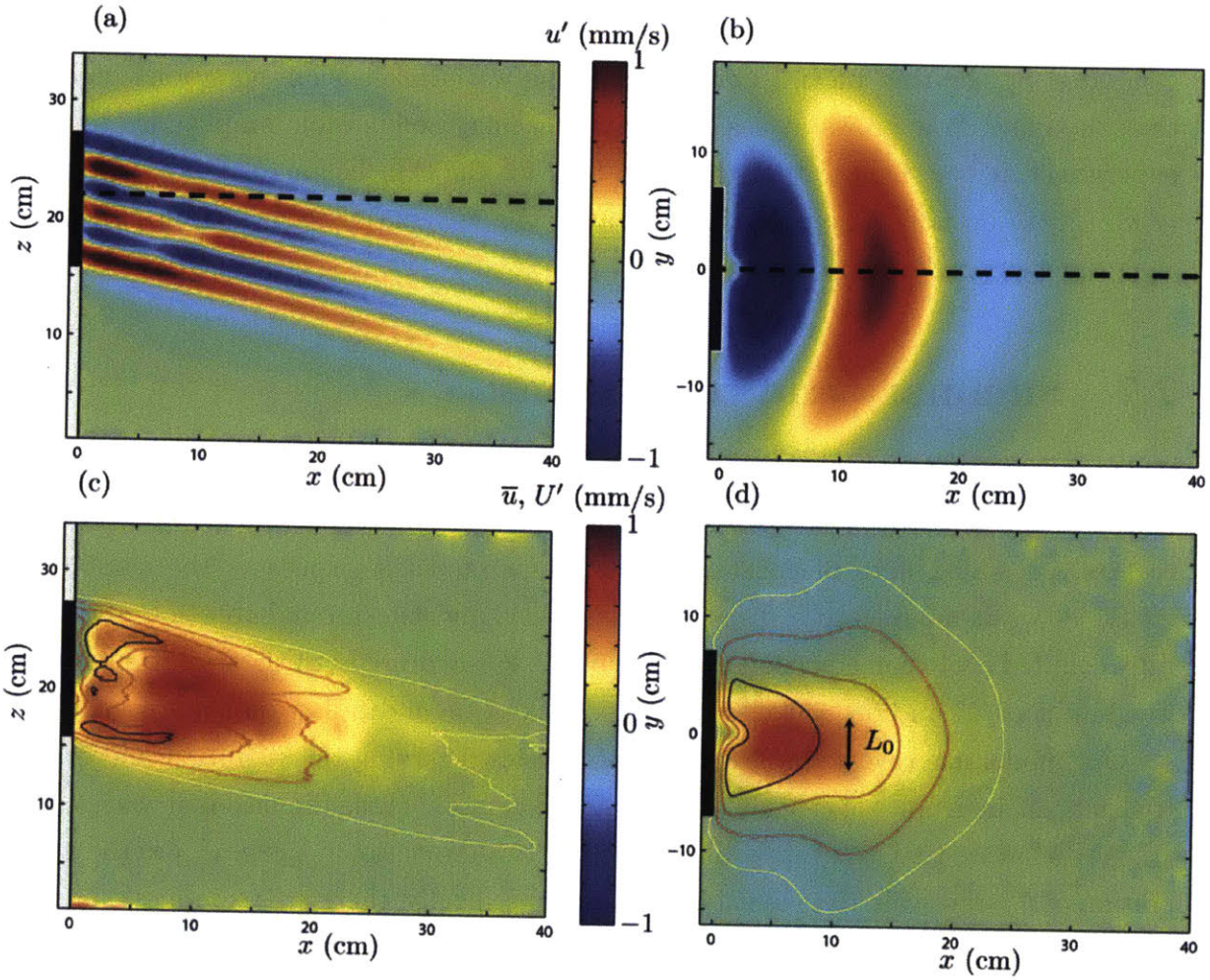

Figure 2-3: Reproduced from Bordes *et al.* (2012), plots show the experimentally measured x-component of the velocity field. Note that the experiment uses z for the vertical and y for the transverse coordinate, while we use the reverse convention. (a) and (b) show vertical and horizontal slices, respectively, of the primary harmonic (wave) field, while (c) and (d) are of the mean flow. The dashed line in (a) indicates the location of the field of view where (b) and (d) are taken, while the dashed line in (b) indicates the field of view of (a) and (c). The black bar indicates the location of the wavemaker. Contours in (c) and (d) correspond to contours of the wave envelope amplitude.

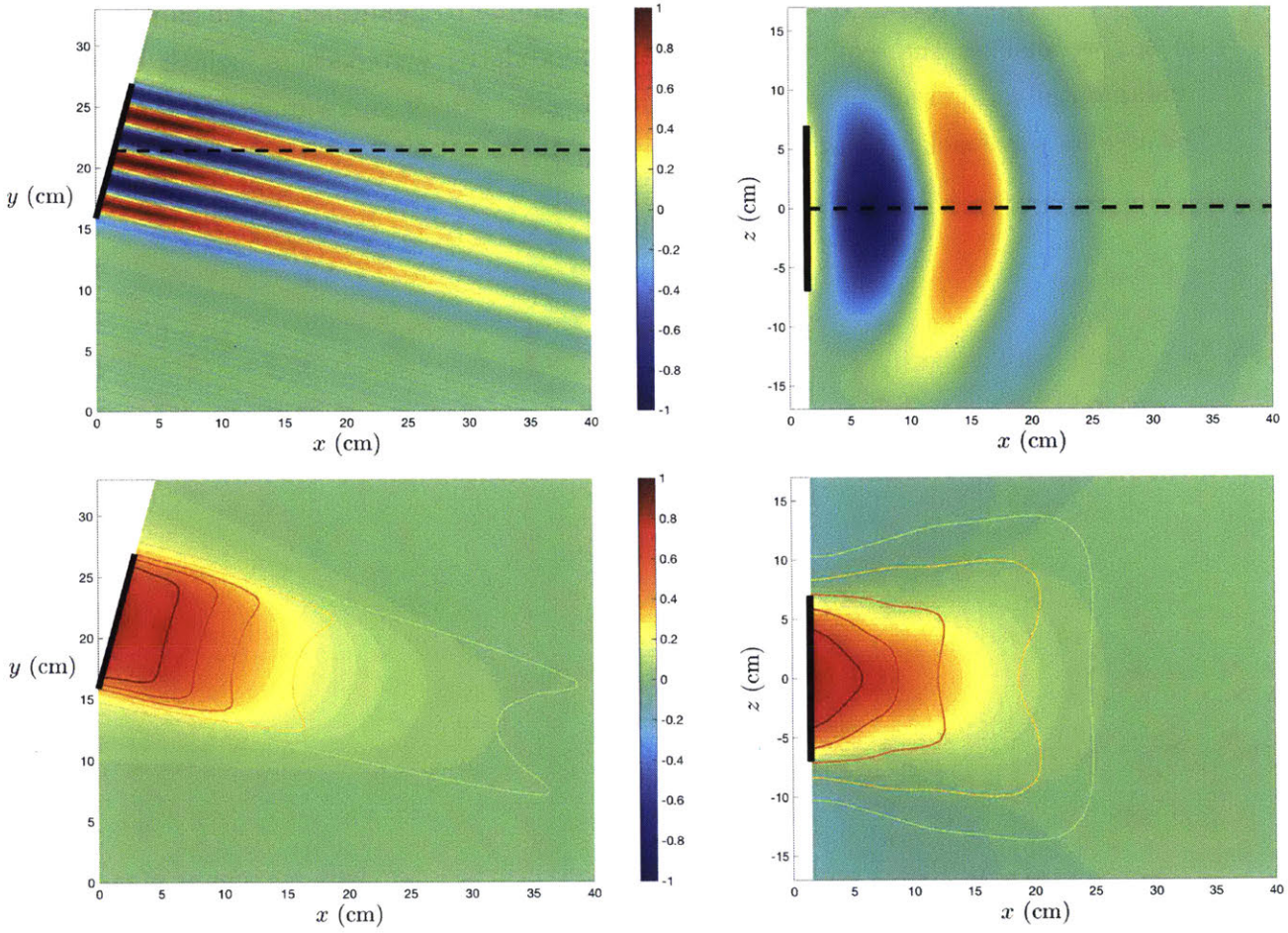

Figure 2-4: Theoretically predicted wave field and mean flow obtained using our wavepacket-beam model by solving (2.19) and (2.26). Plots here are exactly analogous to the plots in figure 2-3, showing the dimensional x-component of the velocity field (in mm/s) at $T = 20$ (dimensional $t = 323$ s). The black bar indicates the approximate location where the boundary condition (2.55) is applied to simulate a wavemaker. Contours in the bottom plots are of the wave envelope amplitude. Note that our model assumes that forcing is directly in the along-beam direction, whereas the experimental wavemaker forces in the horizontal. Nonetheless, we see excellent agreement with the results of Bordes *et al.* (2012).

Regarding the former, we have compared our model against experimental observations and we find excellent agreement.

Thus far, we have discussed many of the novel behaviors exhibited by internal wave beams with three-dimensional variations. In the next Chapter, we turn our attention to what makes these behaviors also unique to beam-like disturbances. To do so, we discuss the evolution of equally modulated wavepackets, which exhibit fundamentally different behavior, and thin beams, which share many of the same features as wavepacket-beams.

Chapter 3

Beam-like versus non-beam-like waves

In the previous chapter, we focused on three-dimensionally modulated wavepacket-beams. In this chapter, we now explore the key role of *modulations* in giving rise to varying types of behavior. Previous studies have focused on horizontal and transverse modulations, e.g. in Sutherland (2001) and Tabaei & Akylas (2007) as discussed in Chapter 1. There, we have already tasted the dramatic effects that differing types of modulations can have on wave behavior, as the flat wavepacket undergoes a 'long-wave–short-wave' resonant interaction that is distinct from the types of wave–mean interactions considered in this thesis.

Thus far, we have seen that transverse modulations are necessary to the generation of a mean flow. However, the roles of along-beam and cross-beam modulations in conjunction with transverse modulations are as of yet unclear. Therefore, we now step away from the wavepacket-beam and consider two other types of internal wave disturbances. In doing so, we show that beam-like internal waves form a general class of internal wave disturbances that exhibit unique properties.

The first system we consider is the three-dimensional equally modulated wavepacket. As compared to the wavepacket-beam, the equally modulated wavepacket features stronger modulations in the along-beam direction. In the inviscid limit, this system has received quite a bit of attention, e.g. in Bretherton (1969) and Shrira (1981) for weakly nonlinear waves, in Grimshaw (1977) for waves in a finite depth ocean, and most recently in Tabaei & Akylas (2007) for finite amplitude waves. However, no study to our knowledge has included fluid dissipation. Here, we consider a viscous (as well as strongly rotating) system and we will show that the strength of viscosity plays a key role in the dynamics of modulated waves.

The second system we consider is the thin beam. As compared to the wavepacket-beam, the thin beam features a locally confined $O(1)$ cross-beam width, i.e. stronger

modulations in the cross-beam direction, as well as general profile rather than nearly monochromatic profile. In the case of no background rotation, this is exactly the system studied by KA in first demonstrating the effects of three-dimensional variations. Here, we extend their analysis by including background rotation.

3.1 Three-dimensional equally modulated wavepackets

Our analysis begins from the governing equations (2.2) and uses the same (ξ, η, z) coordinate system as before. Here, we ignore forcing for simplicity's sake and consider the free propagation of an equally modulated wavepacket. Note that if included, forcing would appear similarly in the reduced equations as in Chapter 2. We also assume strong rotation, $f = O(1)$, but just as in Chapter 2, we find that rotation plays an insignificant role and that the derived evolution equations reduce to the case of no rotation by taking $f = 0$.

We consider a locally confined wavepacket that is weakly modulated in all directions, with carrier wavenumber l and frequency ω_0, thus setting the angle of inclination, θ, via the linear dispersion relation (2.3). To describe the modulations, we employ the envelope variables

$$(X, Y, Z) = \varepsilon(\xi, \eta, z), \tag{3.1}$$

where $0 < \varepsilon \ll 1$ is a small parameter that controls the scale of the modulations. Under these definitions, transverse and cross-beam modulations are of the same scale as in the wavepacket-beam studied in Chapter 2. Now, the only difference is that along-beam modulations are stronger (see figure 3-1 for a schematic).

We again seek a theory in the distinguished limit where leading order nonlinear and dispersive effects balance on the same time scale. Via (2.10), the slow time variable over which leading order dispersive effects act is

$$T = \varepsilon t. \tag{3.2}$$

Next, for weak nonlinearity to act on an $O(\varepsilon^{-1})$ time scale, it turns out that the proper

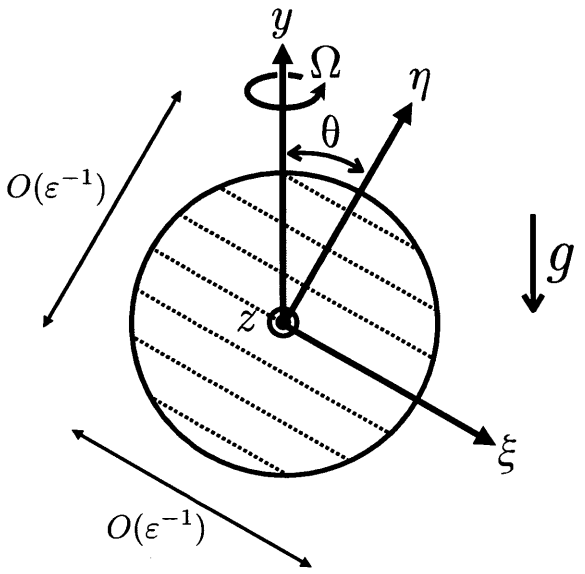

Figure 3-1: Schematic of a three-dimensional equally modulated wavepacket. Dotted lines correspond to the constant phase lines of the sinusoidal carrier, while the bounding solid line corresponds to the finite extent of the slowly varying envelope. As compared to the wavepacket-beam, modulations in the along-beam (ξ-) direction are stronger.

scalings for the flow field primary harmonic and mean components are as follows:

$$u = \varepsilon\{Ue^{i\phi} + \text{c.c.}\} + \varepsilon^2\overline{U} + \ldots, \tag{3.3a}$$

$$v = \varepsilon^2\{Ve^{i\phi} + \text{c.c.}\} + \varepsilon^2\overline{V} + \ldots, \tag{3.3b}$$

$$w = \varepsilon\{We^{i\phi} + \text{c.c.}\} + \varepsilon^2\overline{W} + \ldots, \tag{3.3c}$$

$$\rho = \varepsilon\{Re^{i\phi} + \text{c.c.}\} + \varepsilon^2\overline{R} + \ldots, \tag{3.3d}$$

$$p = \varepsilon\{Pe^{i\phi} + \text{c.c.}\} + \varepsilon\overline{P} + \ldots, \tag{3.3e}$$

where $\phi \equiv l\eta - \omega_0 t$ and all primary harmonic and mean flow amplitudes (U, $\overline{U}$, etc.) are functions of (X, Y, Z, T). We assume that $\nu \ll 1$, but we will specify the scaling of ν in relation to ε later.

Inserting (3.1), (3.2), and (3.3) into our governing equations (2.2), we may once again obtain diagnostic expressions relating all primary harmonic components to the

along-beam wave amplitude, U. These relations, correct to $O(\varepsilon)$, are

$$V = \frac{\mathrm{i}}{l} U_X - \frac{f\cos\theta}{\omega l} U_Z, \tag{3.4a}$$

$$W = \frac{\mathrm{i} f\cos\theta}{\omega} U, \tag{3.4b}$$

$$R = -\frac{\mathrm{i}\sin\theta}{\omega} U, \tag{3.4c}$$

$$P = \frac{1-f^2}{\omega l}\sin\theta\cos\theta\, U. \tag{3.4d}$$

From the mean components, we likewise obtain diagnostic relations between all mean fields and the cross-beam mean velocity component, $\overline{V}$, correct to $O(\varepsilon)$, as

$$\overline{U} = \cot\theta\,\overline{V}, \tag{3.5a}$$

$$\overline{W}_Z = -\overline{V}_Y - \overline{V}_X\cot\theta \tag{3.5b}$$

$$\overline{R}_Z = -f\cot\theta\,\overline{V}_Y + f\overline{V}_X, \tag{3.5c}$$

$$\overline{P}_Z = f\csc\theta\,\overline{V}. \tag{3.5d}$$

Finally, it remains to obtain equations that govern the evolution of U and $\overline{V}$. At this point, it becomes necessary to specify the strength of viscous dissipation, as it will be crucial for the physical implications of the derived evolution equations.

3.1.1 Case of $\nu = O(\varepsilon^2)$

First, we consider the case when $\nu = \beta\varepsilon^2$, as in Chapter 2, where β is an $O(1)$ coefficient. Making use of this scaling, the evolution of U is then given by

$$\boxed{U_T + \frac{(1-f^2)\sin\theta\cos\theta}{\omega_0 l} U_X = 0.} \tag{3.6}$$

We see that viscous effects do not affect evolution over an $O(\varepsilon^{-1})$ time scale. This is not surprising given the proposed scalings and the fact that the viscous attenuation length scale for internal waves is $O(\nu^{-1})$ (Lighthill, 1978).

In order to obtain an evolution equation for $\overline{V}$, we make use of PV evolution as we expect that the mean flow is governed by the mean PV. We find that q can be expanded as

$$q = f + \varepsilon^3\{Qe^{\mathrm{i}\phi} + \text{c.c.}\} + \varepsilon^4\overline{Q} + \ldots, \tag{3.7}$$

where Q and $\overline{Q}$ are $O(1)$ functions of (X, Y, Z, T). Making use of the definition of PV

(2.7), we find that $\overline{Q}$ can be expressed in terms of the velocity field as

$$\overline{Q}_Z \equiv \frac{1}{\sin\theta}\left[\overline{V}_{ZZ} + \omega_0^2\overline{V}_{YY} + (1+f^2-\omega_0^2)\overline{V}_{XX} + 2(1-f^2)\sin\theta\cos\theta\,\overline{V}_{XY}\right] - \frac{2l\sin\theta}{\omega_0}(U^*U)_Z. \quad (3.8)$$

Finally, the PV evolution equation (2.6) gives us that

$$\overline{Q}_T = 0, \quad (3.9)$$

to leading order and assuming no mean flow at $T = 0$, combining (3.9) with (3.8) yields an equation for $\overline{V}$ in terms of U as

$$\boxed{\overline{V}_{ZZ} + \omega_0^2\overline{V}_{YY} + (1+f^2-\omega_0^2)\overline{V}_{XX} + 2(1-f^2)\sin\theta\cos\theta\,\overline{V}_{XY} = \frac{2l\sin^2\theta}{\omega_0}(U^*U)_{ZZ}.} \quad (3.10)$$

Thus, equations (3.6) and (3.10) form a system of equations governing the leading order evolution of the waves and mean flow, respectively.

The most important consequence of these isotropic modulations, immediately seen from (3.6), is that the waves evolve linearly for $t = O(\varepsilon^{-1})$, simply propagating in the along-beam direction at the group velocity $c_g = (1-f^2)\sin\theta\cos\theta/\omega_0 l$. Therefore, while there exists an induced mean flow as described by (3.10), there is no feedback from the mean flow onto the waves. This precludes any possibility of wave instability over this slow time scale. From the mean flow equations, we observe only the existence of the modulation-induced mean flow and no streaming at leading order. While transverse variations are a necessary condition for mean flow generation, this modulation-induced mean exists only in the vicinity of the waves. Taking the limit of no rotation, these equations are equivalent to the expressions derived by Shrira (1981) and Tabaei & Akylas (2007).

One might wonder about the evolution of the equally modulated wavepacket on a longer time scale, specifically when $t = O(\varepsilon^{-2})$, which happens to be the crucial time scale for the wavepacket-beam. By rewriting (3.6) in a reference frame moving with the group velocity, e.g. defining $\tau = X - c_g T$, (3.6) reduces to $U_\tau = 0$. This suggests that nonlinearity may affect the waves over a longer time scale than $O(\varepsilon^{-1})$. While we do not explicitly perform this calculation here, we note that indeed, nonlinear feedback from the induced mean flow arises when $t = O(\varepsilon^{-2})$, suggesting that modulational

instability is possible. Over this longer time scale, the wavepacket is also attenuated by viscosity. However, via (3.10), streaming always remains as a higher order mean flow correction as compared to the purely modulation-induced mean flow.

3.1.2 Case of $\nu = O(\varepsilon)$

Next, we consider the case when $\nu = \beta\varepsilon$, where β is again $O(1)$. Under these flow conditions, the evolution of U is now given by

$$\boxed{U_T + \frac{(1-f^2)\sin\theta\cos\theta}{\omega_0 l}U_X + \frac{\beta_E l^2}{2}U = 0,} \tag{3.11}$$

where β_E is the effective viscosity defined in (2.20). We find that q is now expanded as

$$q = f + \varepsilon^2\{Qe^{i\phi} + \text{c.c.}\} + \varepsilon^3\overline{Q} + \ldots, \tag{3.12}$$

where Q and $\overline{Q}$ are $O(1)$ functions of (X, Y, Z, T). Making use of (2.6), we find that the mean PV is governed by

$$\overline{Q}_T = \frac{2\beta_E l^3 \sin\theta}{\omega_0}(U^*U)_Z + O(\varepsilon) \tag{3.13}$$

and combined with (3.8), which defines the PV in terms of the velocity field, we obtain an evolution equation for $\overline{V}$ as

$$\boxed{\frac{\partial}{\partial T}\left[\overline{V}_{ZZ} + \omega_0^2\overline{V}_{YY} + (1+f^2-\omega_0^2)\overline{V}_{XX} + 2(1-f^2)\sin\theta\cos\theta\,\overline{V}_{XY} - \frac{2l\sin^2\theta}{\omega_0}(U^*U)_{ZZ}\right] = \frac{2\beta_E l^3\sin^2\theta}{\omega_0}(U^*U)_{ZZ}.} \tag{3.14}$$

Compared to the previous case when $\nu = O(\varepsilon^2)$, larger viscosity has dramatic effects. First, we observe from (3.11) that the leading order wave evolution remains linear. However, rather than simply translating at the group velocity, the wavepacket amplitude now undergoes exponential decay as a result of viscosity. This implies that no further dynamics are possible on longer time scales as the wavepacket will have been severely attenuated. Second, we observe from (3.14) that now, both modulation-induced mean flow and streaming arise at leading order in the mean flow equation and that they both rely on three-dimensional variations. However, just as before, no coupling to the waves is permitted and so no instability is possible.

3.1.3 Summary and conclusions

In the preceding analysis, we have shown that while three-dimensional equally modulated wavepackets share some similarities with three-dimensional wavepacket-beams, they exhibit qualitatively different behavior. For both systems, transverse modulations are necessary for mean flow generation.

However, for equally modulated wavepackets, it is not possible for modulation-induced mean flow and streaming to coexist *and* lead to wave instability. First, regardless of the strength of viscous dissipation, wavepacket evolution is linear over a time scale of $O(\varepsilon^{-1})$, thus precluding instability. Second, for $\nu = O(\varepsilon^2)$ and smaller, we note that it is possible for nonlinear mean flow feedback onto the waves, and thus modulational instability, to exist when $t = O(\varepsilon^{-2})$. However, streaming will always be negligible at leading order. Third and finally, for $\nu = O(\varepsilon)$, it is possible for modulation-induced mean flow and streaming to coexist, but neither can cause wave instability as the wavepacket propagates linearly and viscosity causes exponential decay of the wave amplitude over an $O(\varepsilon^{-1})$ time scale.

From this analysis, we draw two major conclusions. First, the relative scales of along-beam modulations and transverse modulations determine whether a disturbance behaves like the wavepacket-beam or like the equally modulated wavepacket. Along-beam modulations dictate the strength of the group velocity effect, i.e. the rate of energy propagation, whereas transverse modulations are crucial to the effects of nonlinearity which drives energy transfer from waves to the mean flow. For beam-like waves, such as the wavepacket-beam, with weaker modulations in the along-beam direction, the effects of dispersion balance nonlinearity, whereas for non-beam-like waves, such as the equally modulated wavepacket, the effect of dispersion dominates over nonlinearity.

Second, if streaming is to be a leading order effect, then waves must be attenuated on the same time scale as they propagate according to the group velocity. In the equally modulated wavepacket, where along-beam modulations are $O(\varepsilon^{-1})$, viscosity must be taken to be $O(\varepsilon)$ for streaming to be a leading order effect. In the case of the wavepacket-beam of Chapter 2, where along-beam modulations are of $O(\varepsilon^{-2})$, viscosity must be accordingly taken to be $O(\varepsilon^2)$.

3.2 Three-dimensional thin beams

While we have just emphasized the role that along-beam modulations play (relative to transverse modulations) and hence the beam-like or non-beam-like nature of the waves, we have not yet considered the role of the cross-beam width and profile. Thus far, we have considered waves that feature locally confined nearly monochromatic cross-beam profile, with an envelope scale of $O(\varepsilon^{-1})$. However, as noted in the introduction, uniform beams with any general cross-beam profile are exact nonlinear solutions. Therefore, it is possible to consider the dynamics of a thin beam, which has locally confined general profile of $O(1)$ width. While the following analysis is more involved than that of the wavepacket-beam, we observe that the two systems share many of the same novel properties.

The thin beam system was considered by KA in the absence of background rotation. Our analysis here extends their model by considering background rotation. This allows us to view all the systems considered in this thesis in the same light. Importantly, it also allows us to determine the applicability and relevance of the model to geophysical contexts. Many field observations (Gerkema *et al.*, 2004; Cole *et al.*, 2009; Johnston *et al.*, 2011) have suggested that the beams generated by tide–topography interactions are in fact thin beams with locally confined profile and cross-beam width of only one or two wavelengths. Therefore, in nature, thin beams are likely to be the most relevant class of internal wave disturbances, as opposed to nearly monochromatic waves. We first focus on the case of $f = O(1)$, and we later make comments on the case of $f = O(\varepsilon)$.

3.2.1 Scalings and inner flow

First, it is necessary to clarify the characteristic length scale, L, used to arrive at the nondimensional governing equations (2.2). In Chapter 2 and § 3.1 where waves had nearly monochromatic profile, we chose the wavelength of the carrier wave in order to establish a theory governing the evolution of the slowly varying envelope. For thin beams of locally confined $O(1)$ width and general profile that varies on an $O(1)$ length scale, there is no separation of scales between carrier and slowly varying envelope. Therefore, for the thin beam, we choose the width of the beam as a characteristic length scale.

In our analysis of a modulated thin beam, we again seek to establish a theory in the distinguished limit, where the effects of rotation, weak nonlinearity, weak dispersion, and weak viscosity balance. To begin, we assume modulations in the transverse

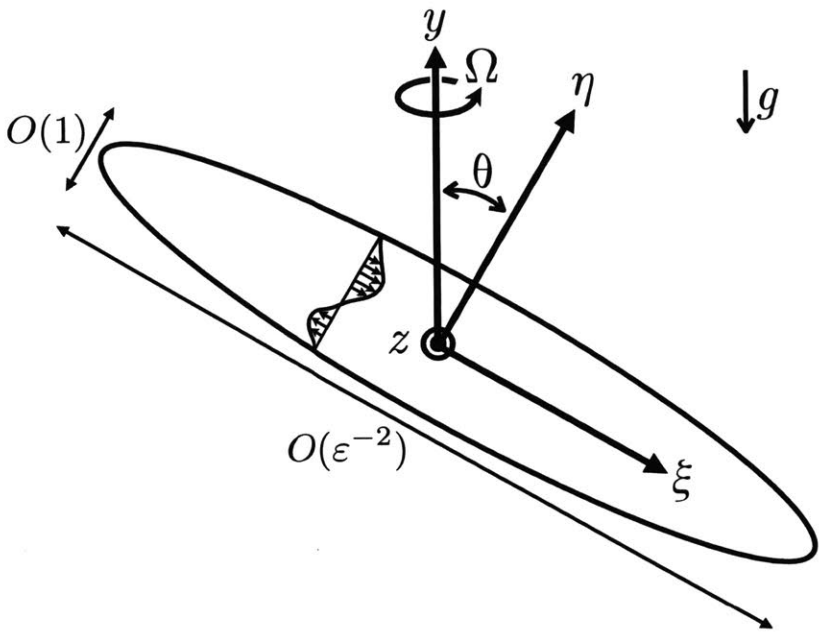

Figure 3-2: Schematic of a thin beam with general profile, where the bounding solid ellipse corresponds to the locally confined nature of the waves.

direction are described by the stretched coordinate,

$$Z = \varepsilon z \quad (0 < \varepsilon \ll 1). \tag{3.15}$$

This brings transverse modulations for all systems considered in this thesis to be of the same order. Via the linear dispersion relation, in order to to balance along-beam and transverse dispersion, it is necessary to take the scales

$$X = \varepsilon^2 \xi, \quad T = \varepsilon^2 t, \tag{3.16}$$

to describe along-beam modulations and slow time respectively. Turning to viscous dissipation, and in consideration of our conclusions from § 3.1, it turns out that for viscosity to attenuate the waves over a time scale of $O(\varepsilon^{-2})$, we must take

$$\nu = \beta \varepsilon^2, \tag{3.17}$$

where β is an $O(1)$ coefficient. We note that thus far, this analysis is identical to that for the wavepacket-beam in Chapter 2, and that for the thin beam under no background rotation (KA).

Next, it remains to link the forcing amplitude to the modulation scale, hence

balancing weak nonlinearity with dispersion and viscous dissipation. It turns out that for weak nonlinearity to act such that the induced mean flow evolves when $T = O(1)$, it is necessary to take the amplitude of forcing, and thus the beam amplitude, to be $O(\varepsilon^{1/2})$. Accordingly, in the far field where the forcing in the along-beam direction appears as a delta function, the forcing is taken to be

$$F \to 2\varepsilon^{5/2}\delta(X)\{f(\eta, Z)e^{-\mathrm{i}\omega_0 t} + \text{c.c.}\}, \quad H \to 2\varepsilon^{5/2}\delta(X)\{h(\eta, Z)e^{-\mathrm{i}\omega_0 t} + \text{c.c.}\}. \tag{3.18}$$

At this point, we note that the scalings have differed from those in Chapter 2, although they remain identical to those in KA. Finally, to describe the wave–mean interaction under the presence of background rotation, we expand the the flow field as follows:

$$u = \varepsilon^{1/2}\{Ue^{-\mathrm{i}\omega_0 t} + \text{c.c.}\} + \varepsilon^2\overline{U} + \ldots, \tag{3.19a}$$

$$v = \varepsilon^{3/2}\{Ve^{-\mathrm{i}\omega_0 t} + \text{c.c.}\} + \varepsilon^2\overline{V}_\infty(X, Z, T) + \varepsilon^3\overline{V} + \ldots, \tag{3.19b}$$

$$w = \varepsilon^{1/2}\{We^{-\mathrm{i}\omega_0 t} + \text{c.c.}\} + \varepsilon^2\overline{W} + \ldots, \tag{3.19c}$$

$$\rho = \varepsilon^{1/2}\{Re^{-\mathrm{i}\omega_0 t} + \text{c.c.}\} + \varepsilon^2\overline{R} + \ldots, \tag{3.19d}$$

$$p = \varepsilon^{1/2}\{Pe^{-\mathrm{i}\omega_0 t} + \text{c.c.}\} + \varepsilon\overline{P}_\infty(X, Z, T) + \varepsilon^2\overline{P} + \ldots, \tag{3.19e}$$

where all primary harmonic and mean amplitudes, unless otherwise specified, are functions of (X, η, Z, T). Importantly, $\overline{V}_\infty$ and $\overline{P}_\infty$ are independent of η, implying that they are constant in the cross-beam direction. Looking ahead, the presence of these constant flow components will later necessitate a matched-asymptotics procedure to fully determine the wave–mean flow dynamics. This will be necessary because these constant flow components extend far away from the vicinity of the locally confined waves and therefore cannot satisfy boundary conditions, implying that we will need to rescale the flow field far away from the beam ($|\eta| \gg 1$). Thus, the scalings (3.19) only apply to the inner flow in the vicinity of the beam where $\eta = O(1)$. Later, we will discuss scalings for the outer flow where $|\eta| \gg 1$. At this point, we note that our analysis has diverged from that of the thin beam with no background rotation as a result of the scalings (3.19).

Now, we may deduce the dynamics of the wave–mean interaction in the near vicinity of the beam. Inserting (3.19) into our governing equations and gathering terms that contribute to the evolution of the primary harmonic yields diagnostic

relations between all primary harmonic flow fields and U, namely

$$V = -\mathrm{i}\frac{f\cos\theta}{\omega_0}\int^{\eta} U_Z \,\mathrm{d}\eta', \tag{3.20a}$$

$$W = \mathrm{i}\frac{f\cos\theta}{\omega_0}U, \tag{3.20b}$$

$$R = -\mathrm{i}\frac{f\sin\theta}{\omega_0}U, \tag{3.20c}$$

$$P = \mathrm{i}\frac{(1-f^2)\sin\theta\cos\theta}{\omega_0}\int^{\eta} U \,\mathrm{d}\eta', \tag{3.20d}$$

to leading order. Making use of these relations, we obtain at leading order an evolution equation for U as

$$\boxed{U_T + \overline{V}_\infty U_\eta + \mathrm{i}\frac{(1-f^2)}{\omega_0}\sin\theta\cos\theta\Big[\int^{\eta} U_X \,\mathrm{d}\eta' + \frac{\cot\theta}{2}\int^{\eta}\int^{\eta'} U_{ZZ}\,\mathrm{d}\eta''\,\mathrm{d}\eta'\Big] - \frac{\beta_E}{2}U_{\eta\eta} = \delta(X)f,} \tag{3.21}$$

where β_E is the effective viscosity given by (2.20). As expected, the evolution of the waves for a thin beam is similar to that of the wavepacket-beam (2.19) and in fact, (3.21) reduces to (2.19) if a monochromatic cross-beam profile is assumed. This is because the width of the cross-beam profile plays no role in the leading order linear evolution of slowly modulated internal waves, as can be seen from (2.10). From (3.21), we also note that strong rotation again plays a minor role in wave evolution. As we showed in § 2.4, for a fixed forcing frequency, rotation only affects the coefficients in front of the group velocity effect of along-beam modulations and viscosity, and does not affect transverse dispersion.

Similarly to the wavepacket-beam, feedback of the induced mean flow onto the waves is felt though the cross-beam mean flow component. In light of the results from § 3.1, we note that it is precisely because of the beam-like nature of these waves that nonlinearity affects wave evolution at leading order. For the case of the equally modulated wavepacket, an example of a non-beam-like wave disturbance, nonlinearity does not affect wave evolution at leading order. One key difference that can be seen here between the wavepacket-beam and the thin beam is that for the thin beam, the induced mean feedback component, $\overline{V}_\infty$ is constant in the cross-beam direction and thus extends far away from the beam itself.

Gathering the mean components, we may first diagnostically relate all flow fields

to $\overline{V}_\infty$ and $\overline{W}$ as follows:

$$\overline{U} = \cot\theta\,\overline{V}_\infty + \frac{f\cos\theta}{\omega_0^2}\Big\{J(U^*, \textstyle\int^\eta U\,\mathrm{d}\eta') + \text{c.c.}\Big\}, \tag{3.22a}$$

$$\overline{V} = -\int^\eta \overline{W}_Z\,\mathrm{d}\eta', \tag{3.22b}$$

$$\overline{R} = f\cot\theta\,\overline{W} + \frac{f\cot\theta}{\omega_0}\Big\{\mathrm{i}J(U^*, \textstyle\int^\eta U\,\mathrm{d}\eta') + \text{c.c.}\Big\}, \tag{3.22c}$$

$$\overline{P} = -f\sin\theta\,\overline{W} - \cos\theta\,\overline{R}, \tag{3.22d}$$

$$\overline{P}_{\infty Z} = f\csc\theta\,\overline{V}_\infty, \tag{3.22e}$$

where $J(A,B) \equiv A_\eta B_Z - B_\eta A_Z$ stands for the Jacobian. Here, of all the systems studied in this thesis, a feature unique to only the thin beam with strong rotation is that mean flow is non-hydrostatic. Via (3.22a), we see that a non-horizontal component of the mean flow arises in the vicinity of the waves that is the result of nonlinearity and strong rotation. At this point, we observe a complication that arises in the thin beam that does not arise in the wavepacket-beam. In addition to $\overline{V}_\infty$ being undetermined, we were not able to eliminate $\overline{W}$ via diagnostic relations as we were able to for the wavepacket-beam.

Anticipating that the mean flow response will be governed by the evolution of mean PV, we now turn to PV evolution. It turns out that the PV field may be expanded into primary harmonic and mean components as

$$q = f + \varepsilon^{5/2}\big\{Qe^{-\mathrm{i}\omega_0 t} + \text{c.c.}\big\} + \varepsilon^2\overline{Q} + \ldots, \tag{3.23}$$

where Q and $\overline{Q}$ are $O(1)$ functions of (X,η,Z,T). Via (2.6), the primary harmonic component of the PV can be expressed in terms of U as

$$Q = \beta\frac{f\sin\theta\cos\theta}{\omega_0^2}U_{\eta\eta\eta} + O(\varepsilon), \tag{3.24}$$

while the evolution of the mean PV is given by,

$$\begin{aligned}\overline{Q}_T + \overline{V}_\infty\overline{Q}_\eta = {}& -\beta\sin\theta\,\overline{W}_{\eta\eta\eta} \\ & - \beta\frac{\sin\theta}{\omega_0}\Big\{\mathrm{i}J(U^*_{\eta\eta}, U) + \mathrm{i}\frac{f^2\cos^2\theta}{\omega_0^2}J(U^*_{\eta\eta\eta}, \textstyle\int^\eta U\,\mathrm{d}\eta') + \text{c.c.}\Big\}.\end{aligned} \tag{3.25}$$

Just as in the wavepacket-beam, we see that mean PV is produced by nonlinear, viscous effects. In order to obtain a single evolution equation for $\overline{W}$, we use (2.7) to

write $\overline{Q}$ in terms of the velocity field as

$$\overline{Q} = -\frac{\omega_0^2}{\sin\theta}\overline{W}_\eta - \frac{\sin\theta}{\omega_0}\Big\{\mathrm{i}J(U^*,U) - \mathrm{i}f^2\cot^2\theta\frac{\partial}{\partial\eta}J(U^*,\textstyle\int^\eta U\,\mathrm{d}\eta') + \mathrm{c.c.}\Big\}. \tag{3.26}$$

Inserting (3.26) into (3.25), it is now possible to derive a single equation coupling the evolution of $\overline{W}$ and U, although we do not explicitly write it here due to its length. This equation is analogous to equation (3.10) in KA.

To summarize, we have thus far derived two evolution equations. The first, (3.21), is an evolution equation coupling U to the induced mean flow $\overline{V}_\infty$. The second, the one mentioned in the previous paragraph but not explicitly stated, is an evolution equation coupling $\overline{W}$ to U. At this point, we must still relate the unknown $\overline{V}_\infty$ back to U or $\overline{W}$ in order to obtain a closed system. To this end, it is now useful to examine the boundary conditions which our system must satisfy.

3.2.2 Outer flow and asymptotic matching

As we have assumed forcing that is locally confined in η, we expect our solution to satisfy the boundary condition

$$(\boldsymbol{u},\rho,p) \to 0 \qquad (\eta \to \pm\infty). \tag{3.27}$$

Examining our primary harmonic flow field (3.20), this implies that U must satisfy

$$\int^\eta\int^{\eta'} U\,\mathrm{d}\eta''\,\mathrm{d}\eta' \to 0 \qquad (\eta \to \pm\infty). \tag{3.28}$$

However, turning to the mean flow components, we may deduce that they cannot possibly satisfy these boundary conditions. First and foremost, $\overline{V}_\infty$ is constant in the cross-beam direction and (3.22a) implies that $\overline{U}$ does not vanish either. In addition, from (3.26), $\overline{Q} \sim \overline{W}_\eta$, implying that even if $\overline{Q}$ vanishes at infinity, $\overline{W}$ may instead go to constant non-zero values. In fact, we may explicitly calculate the values of $\overline{W}$ at infinity by integrating (3.25) and (3.26) over the cross-beam domain. This gives us that

$$\overline{W}_T\Big|_{\eta\to-\infty}^{\eta\to\infty} = \mathrm{i}\frac{2\sin^2\theta}{\omega_0^3}\frac{\partial}{\partial Z}\int_{-\infty}^{\infty}\Big\{(U^*U_\eta)_T + \beta_E U_\eta^* U_{\eta\eta}\Big\}\,\mathrm{d}\eta\,. \tag{3.29}$$

Note that this expression will be later useful in the asymptotic matching procedure. At this point, it is clear that our inner flow scalings and solution are not uniformly valid and we must rescale our flow field far away from the beam. There, we must solve

an outer flow equation whose solution must then be smoothly joined to the inner flow solution.

In order to determine the appropriate scalings for the outer flow ($|\eta| \gg 1$), let us denote the values of $\overline{W}$ far away from the beam as

$$\overline{W}(X,\eta,Z,T) \to \overline{W}_{\pm\infty}(X,Z,T) \qquad (|\eta| \gg 1) \tag{3.30}$$

Via (3.22), it follows that for $|\eta| \gg 1$, the other mean flow components scale as the following:

$$\overline{V} \sim \eta \frac{\partial \overline{W}_{\pm\infty}}{\partial Z}, \tag{3.31a}$$

$$\overline{U} \sim \cot\theta\, \overline{V}_{\infty}. \tag{3.31b}$$

Thus, (3.31a) implies that far from the vicinity of the beam, the asymptotic expansion for v in (3.19) breaks down, as the higher order mean flow component $\overline{V}$ becomes comparable to $\overline{V}_{\infty}$ when $\eta = O(\varepsilon^{-1})$. Next, (3.31b) implies that the mean flow far from the beam is horizontal to leading order. Therefore, far away from the beam, where the wave amplitude has vanished, the flow field consists of only mean components and scales as

$$\boldsymbol{u} \sim \varepsilon^2 \Big\{ (\cot\theta\, \overline{V}_{\infty}, \overline{V}_{\infty}, \overline{W}_{\pm\infty}) + O(\varepsilon\eta) \Big\}. \tag{3.32}$$

Based on these scaling arguments and in order for the inner solution to smoothly join to the outer solution, this immediately suggests an outer flow where the flow field is scaled as

$$\boldsymbol{u} = \varepsilon^2(\tilde{U},\tilde{V},\tilde{W}), \qquad \rho = \varepsilon^2 \tilde{R}, \qquad p = \varepsilon \tilde{P}, \tag{3.33}$$

and all fields are functions of (X,Y,Z,T) where

$$Y = \varepsilon\eta, \tag{3.34}$$

is a stretched cross-beam coordinate. Inserting this rescaled flow field into our governing equations, we may now solve for the outer flow field. First, we obtain that

$$\tilde{W}_Z = -\tilde{V}_Y, \qquad \tilde{U} = \cot\theta\, \tilde{V}, \tag{3.35}$$

and eliminating all variables in favor of $\tilde{V}$, it turns out that the outer flow is governed

by a single equation, which to leading order, is

$$\frac{\partial}{\partial T}\left(\tilde{V}_{ZZ}+\omega_0^2\tilde{V}_{YY}\right)=0. \tag{3.36}$$

This equation must now be solved subject to the boundary condition

$$(\tilde{U},\tilde{V},\tilde{W})\to(\cot\theta\,\overline{V}_\infty,\overline{V}_\infty,\overline{W}_{\pm\infty})\qquad(Y\to 0^{\pm}), \tag{3.37}$$

in order to join smoothly with the inner flow, as well as the general boundary condition (3.27) that the flow must vanish as $Y\to\pm\infty$. We note that (3.36) exactly corresponds to a statement about the material conservation of PV in the outer flow. This can be easily verified by inserting the scalings (3.33) into the equations governing PV, (2.6) and (2.7).

We now solve for the outer flow. Assuming that there is no mean flow at $T=0$, (3.36) can be trivially integrated in time and the resulting Laplace equation may be solved by taking Fourier transforms. The resulting solution for the outer flow velocity field is

$$(\tilde{U},\tilde{V},\tilde{W})=\begin{cases}(\cot\theta,1,-\frac{\mathrm{i}}{\omega_0})\int_0^\infty \hat{V}_\infty e^{\mathrm{i}mZ}e^{-mY/\omega_0}\,\mathrm{d}m+\text{c.c.} & (Y>0)\\ (\cot\theta,1,\frac{\mathrm{i}}{\omega_0})\int_0^\infty \hat{V}_\infty e^{\mathrm{i}mZ}e^{mY/\omega_0}\,\mathrm{d}m+\text{c.c.} & (Y<0)\end{cases}, \tag{3.38}$$

where

$$\hat{V}_\infty=\frac{1}{2\pi}\int_{-\infty}^{\infty}\overline{V}_\infty e^{-\mathrm{i}mZ}\,\mathrm{d}Z\,, \tag{3.39}$$

denotes the Fourier transform in Z. Here, we observe two properties of the outer flow. First, via (3.35), it is a purely horizontal flow. Second, it has no time evolution of its own and is 'slaved' to the inner flow via $\overline{V}_\infty$, which manifests as a boundary (matching) condition in the cross-beam direction.

Note that (3.38) has only made use of the cross-beam matching condition from (3.40) and automatically satisfies the along-beam matching condition. Now, imposing the matching condition in the transverse direction, we obtain that

$$\begin{aligned}\overline{W}_{\pm\infty}&=\tilde{W}\Big|_{Y=0^{\pm}}\\ &=\mp\frac{\mathrm{i}}{\omega_0}\int_0^\infty \hat{V}_\infty e^{\mathrm{i}mZ}\,\mathrm{d}m+\text{c.c.}\\ &=\mp\frac{1}{\omega_0}\mathscr{H}[\overline{V}_\infty],\end{aligned} \tag{3.40}$$

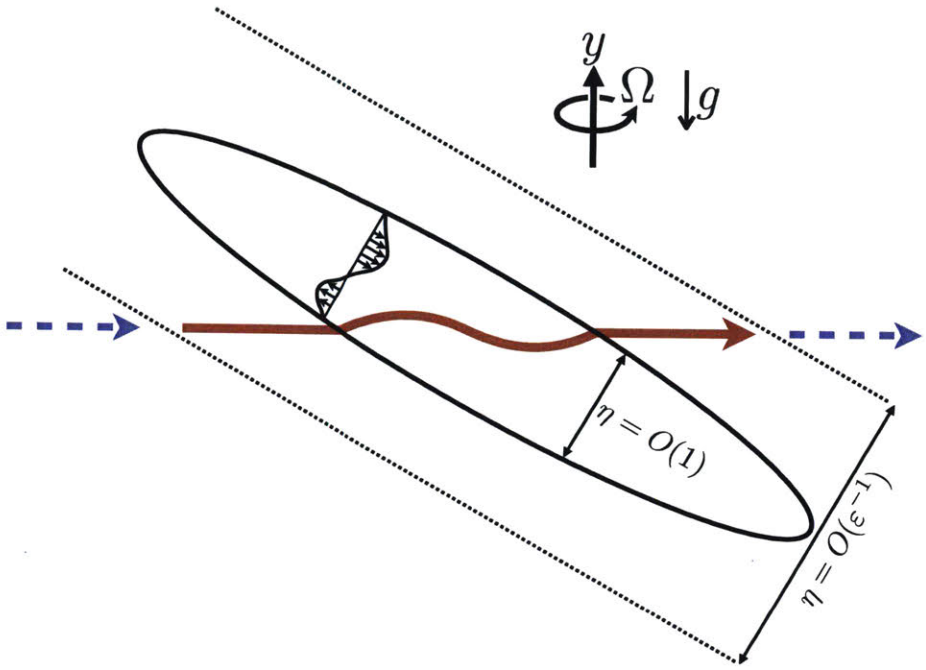

Figure 3-3: Geometry of the inner and outer flows for the three-dimensional modulated thin beam system. Locally confined extent of the beam is indicated by the solid black ellipse and has $O(1)$ cross-beam width. In the inner flow, where $\eta = O(1)$, the induced mean flow (solid red arrow) extends far from the waves. This inner mean flow is predominately horizontal, except for a small non-hydrostatic component in the vicinity of the waves that arises from strong background rotation. In the outer flow, where $\eta = O(\varepsilon^{-1})$, the induced mean flow (blue dotted arrows) is horizontal, slaved to the inner flow, and decays to zero at infinity.

where

$$\mathscr{H}[\overline{V}_\infty] = \int_{-\infty}^{\infty} \mathrm{i}\,\mathrm{sgn}(m)\hat{V}_\infty e^{\mathrm{i}mZ}\,\mathrm{d}m \tag{3.41}$$

denotes the Hilbert transform in Z. Finally, as we have already obtained an equation relating $\overline{W}_{\pm\infty}$ to U in (3.29), we can now use the matching condition (3.40) to relate $\overline{V}_\infty$ to U, thereby closing our system of evolution equations. Combining (3.40) with (3.29), we arrive at the final evolution equation that relates $\overline{V}_\infty$ with U as

$$\boxed{\frac{\partial \overline{V}_\infty}{\partial T} = \mathrm{i}\frac{\sin^2\theta}{\omega_0^2}\frac{\partial}{\partial Z}\mathscr{H}\left[\int_{-\infty}^{\infty}\left\{(U^*U_\eta)_T + \beta_E U_\eta^* U_{\eta\eta}\right\}\mathrm{d}\eta\right].} \tag{3.42}$$

This equation and (3.21) form a coupled system of evolution equations that describe the wave–mean interaction.

As can be seen from the coupled evolution equations (3.21) and (3.42), the dynam-

ics of thin beams share many similar properties with the dynamics of wavepacket-beams discussed in Chapter 2. First, three-dimensional modulations are necessary in triggering an induced mean flow through the action of Reynold stresses. Second, two types of mean flow generation mechanisms exist and operate on the same slow time scale: an inviscid purely modulation-induced mechanism as well as a viscous mechanism that results in streaming and resonant mean flow growth. Importantly, the mean flow feeds back into the waves via nonlinearity at leading order, similarly to the wavepacket-beam and in contrast to the equally modulated wavepacket.

As streaming results in obvious wave distortion, it remains to comment on the effect of the inviscid modulation-induced mean flow on beam stability. To do so, we note that just as in the case of the wavepacket-beam, rotation affects the wave–mean dynamics of thin beams only in the coefficients of the resulting equations and not their form. Therefore, we conclude that the same stability results of Kataoka & Akylas (2013) and Kataoka & Akylas (2016), which were obtained in the non-rotating system, also apply to the rotating system. Specifically, it is possible for the modulation-induced mean flow to trigger a modulational instability for both progressive waves and standing waves, depending on wave amplitude and the exact wave profile. Thus, both types of mean flows are capable of dramatically distorting thin beams in rotating systems, just as in the case of the wavepacket-beam.

3.2.3 Case of weak rotation

For completeness, we may deduce the effect of weak rotation by following a similar analysis with $f = O(\varepsilon)$. Rescaling $f \to \varepsilon f$ and employing the same modulation scales as before, the modified inner flow primary–mean expansion scalings for a thin beam under weak background rotation are taken to be

$$u = \varepsilon^{1/2}\{Ue^{-\mathrm{i}\omega_0 t} + \text{c.c.}\} + \varepsilon^2\overline{U} + \ldots, \tag{3.43a}$$

$$v = \varepsilon^{5/2}\{Ve^{-\mathrm{i}\omega_0 t} + \text{c.c.}\} + \varepsilon^2\overline{V}_\infty(X, Z, T) + \varepsilon^3\overline{V} + \ldots, \tag{3.43b}$$

$$w = \varepsilon^{3/2}\{We^{-\mathrm{i}\omega_0 t} + \text{c.c.}\} + \varepsilon^2\overline{W} + \ldots, \tag{3.43c}$$

$$\rho = \varepsilon^{1/2}\{Re^{-\mathrm{i}\omega_0 t} + \text{c.c.}\} + \varepsilon^3\overline{R} + \ldots, \tag{3.43d}$$

$$p = \varepsilon^{1/2}\{Pe^{-\mathrm{i}\omega_0 t} + \text{c.c.}\} + \varepsilon^2\overline{P}_\infty(X, Z, T) + \varepsilon^3\overline{P} + \ldots, \tag{3.43e}$$

Following a very similar inner/outer flow analysis as before, we obtain coupled equations in the inner flow governing the along-beam wave amplitude as

$$U_T + \overline{V}_\infty U_\eta + \mathrm{i}\cos\theta\Big[\int^\eta U_X\,\mathrm{d}\eta' + \frac{\cot\theta}{2}\int^\eta\int^{\eta'} U_{ZZ}\,\mathrm{d}\eta''\,\mathrm{d}\eta'\Big] - \frac{\beta}{2}U_{\eta\eta} + \mathrm{i}\frac{f^2\cos^2\theta}{2\sin^2\theta}U = \delta(X)f. \quad (3.44)$$

and the cross-beam mean flow as

$$\frac{\partial\overline{V}_\infty}{\partial T} = \mathrm{i}\frac{\partial}{\partial Z}\mathscr{H}\left[\int_{-\infty}^{\infty}\left\{(U^*U_\eta)_T + \beta U_\eta^* U_{\eta\eta}\right\}\mathrm{d}\eta\right]. \quad (3.45)$$

Just as in the case of the wavepacket-beam, weak background rotation only affects wave evolution and not the mean flow, and amounts solely to a small frequency shift in the waves.

3.2.4 Summary and conclusions

In this section, we have discussed the dynamics of three-dimensional modulated thin beams in a rotating stratified fluid. For both thin beams and wavepacket-beams, three-dimensional modulations and nonlinearity trigger an induced mean flow. For both systems, modulation-induced mean flow and streaming coexist and and may each result in wave instability and breakdown. This latter point is the key distinguishing feature for beam-like waves as compared to the equally modulated wavepacket.

For multiple reasons, the analysis of the thin beam is much more difficult than that of the wavepacket-beam, both theoretically and computationally. First, in the thin beam, as the mean flow extends far away from the vicinity of beam, we see that a matched-asymptotics procedure is necessary. In the wavepacket-beam, no such matching between an inner and outer flow is necessary as the mean flow extends over the same cross-beam width as the waves. Second, while (3.21) and (3.42) capture the weakly nonlinear dynamics of the thin beam, including the feedback of the induced mean flow, they are not sufficient to obtain the full flow field. We must additionally solve the evolution equation that governs $\overline{W}$ given by (3.25) and (3.26). In the wavepacket-beam, this was not necessary as the two coupled evolution equations (2.19) and (2.26) are sufficient to determine the entire flow field.

Finally, it is worthwhile to note a few differences between the thin beam and the wavepacket-beam. First, the wavepacket-beam can be considered more unstable to

three-dimensional modulations. This is because an $O(\varepsilon)$ amplitude wavepacket-beam generates the same $O(\varepsilon^2)$ mean flow as an $O(\varepsilon^{1/2})$ thin beam. In both cases, the induced mean flow extends over an $O(\varepsilon^{-1})$ cross-beam width. Thus, while the cross-beam width and profile do not qualitatively affect the induced mean flow phenomena, they play a important role in the strength of the mean flow relative to the waves. Second, we note that if background rotation is strong, the mean flow in the vicinity of the thin beam includes a non-hydrostatic component, in contrast to all other systems considered in this thesis where the mean flow is purely hydrostatic.

THIS PAGE INTENTIONALLY LEFT BLANK

Chapter 4

Concluding remarks

We have studied various internal wave systems in an effort to understand the role of three-dimensional variations in nonlinear wave evolution. For all the systems considered, we have shown that *three-dimensional variations are crucial* in triggering the transfer of energy from waves to an induced mean flow via Reynolds stresses. Two-dimensional models fail to capture these physically relevant dynamics. More specifically, there are *two distinct mechanisms* by which these mean flows are generated. One derives purely from three-dimensional modulations of a uniform state and is an inviscid mechanism. The other relies on both three-dimensional modulations and viscosity, resulting in a phenomena known as streaming where the mean flow grows resonantly. Our derived evolution equations capture these unique features of three-dimensional internal waves and indicate that large-scale induced mean flows may be central to internal wave dynamics.

However, no matter the novelty of these induced mean flows, their mere existence is only a part of the story. We originally sought to understand how these induced mean flows in turn affect wave evolution. Could they could help predict eventual wave dissipation? It is to this end that we drew the distinction between beam-like disturbances, i.e. the wavepacket-beam and thin beam, and non-beam-like disturbances, of which we chose the equally modulated wavepacket as an example. We observe that beam-like waves have the unique property that modulation-induced mean flow and streaming coexist and each may independently lead to wave instability. This is not the case for the equally modulated wavepacket, where nonlinear effects turn out to be negligible at leading order. Therefore, for beam-like waves, *wave instability via induced mean flows* may be central to their evolution. As a result of the coexistence of modulation-induced mean flows and streaming, our results for modulated wave beams may be applicable in both geophysical and laboratory settings. In geophysical

contexts, where waves propagate nearly inviscidly, modulational instability may be an important factor leading to wave breakdown. In the laboratory, where viscosity plays a much larger role, streaming may instead emerge as the dominant phenomena.

A few other key results must also be stressed. First, three-dimensional variations trigger the transfer of energy from waves to a balanced mean flow that is associated with the mean PV. While the modulation-induced mean flow is associated with the material conversation of PV, streaming arises via irreversible transport of PV via viscous dissipation. Second, in order for streaming to arise as a leading order effect, waves must be attenuated on the same order as the group velocity effect (see § 3). Third and finally, background rotation plays a minor role in the wave–mean interaction, at most affecting the coefficients of the various terms in derived evolution equations. This has been demonstrated by considering both strong, $f = O(1)$, and weak, $f \ll 1$, rotation.

While this thesis sheds light on the role of induced mean flows as an important pathway for internal wave instability, we have ignored the effects of the other major pathway, namely the triadic resonance instability (e.g. PSI). Which of the two pathways is dominant and in what circumstances? These important questions remain unanswered and are fundamental in our understanding of internal wave dynamics both in nature and in the laboratory.

Bibliography

BELL, T. H. 1975 Lee waves in stratified flows with simple harmonic time dependence. *Journal of Fluid Mechanics* **67**, 705–722.

BORDES, GUILHEM, VENAILLE, ANTOINE, JOUBAUD, SYLVAIN, ODIER, PHILIPPE & DAUXOIS, THIERRY 2012 Experimental observation of a strong mean flow induced by internal gravity waves. *Physics of Fluids* **24** (8).

BOURGET, BAPTISTE, DAUXOIS, THIERRY, JOUBAUD, SYLVAIN & ODIER, PHILIPPE 2013 Experimental study of parametric subharmonic instability for internal plane waves. *Journal of Fluid Mechanics* **723**, 1–20.

BOURGET, BAPTISTE, SCOLAN, HÉLÈNE, DAUXOIS, THIERRY, LE BARS, MICHAEL, ODIER, PHILIPPE & JOUBAUD, SYLVAIN 2014 Finite-size effects in parametric subharmonic instability. *Journal of Fluid Mechanics* **759**, 739–750.

BRETHERTON, FRANCIS P. 1969 On the mean motion induced by internal gravity waves. *Journal of Fluid Mechanics* **36** (4), 785–803.

CLARK, HEATHER A. & SUTHERLAND, BRUCE R. 2010 Generation, propagation, and breaking of an internal wave beam. *Physics of Fluids* **22** (7), –.

COLE, S. T., RUDNICK, D. L., HODGES, B. A. & MARTIN, J. P. 2009 Observations of tidal internal wave beams at kauai channel, hawaii. *Journal of Physical Oceanography* **39** (2), 421–436.

DAUXOIS, T., JOUBAUD, S., ODIER, P. & VENAILLE, A. 2018 Instabilities of internal gravity wave beams. `arXiv:1702.07762`.

ECHEVERRI, PAULA & PEACOCK, THOMAS 2010 Internal tide generation by arbitrary two-dimensional topography. *Journal of Fluid Mechanics* **659**, 247–266.

GARRETT, CHRIS 2003 Internal tides and ocean mixing. *Science* **301** (5641), 1858–1859, arXiv: http://science.sciencemag.org/content/301/5641/1858.full.pdf.

GARRETT, CHRIS & KUNZE, ERIC 2007 Internal tide generation in the deep ocean. *Annual Review of Fluid Mechanics* **39** (1), 57–87.

GERKEMA, THEO, LAM, FRANS-PETER A. & MAAS, LEO R. M. 2004 Internal tides in the bay of biscay: conversion rates and seasonal effects. *Deep Sea Research Part II: Topical Studies in Oceanography* **51** (25–26), 2995–3008.

GOSTIAUX, L., DIDELLE, H., MERCIER, S. & DAUXOIS, T. 2007 A novel internal waves generator. *Experiments in Fluids* **42** (1), 123–130.

GRIMSHAW, R. H. J. 1977 The modulation of an internal gravity-wave packet, and the resonance with the mean motion. *Studies in Applied Mathematics* **56** (3), 241–266.

GRISOUARD, NICOLAS & BÜHLER, OLIVER 2012 Forcing of oceanic mean flows by dissipating internal tides. *Journal of Fluid Mechanics* **708**, 250–278.

GRISOUARD, NICOLAS, LECLAIR, MATTHIEU, GOSTIAUX, LOUIS & STAQUET, CHANTAL 2013 Large scale energy transfer from an internal gravity wave reflecting on a simple slope. *Procedia {IUTAM}* **8**, 119 – 128.

JOHNSTON, T. M. SHAUN, RUDNICK, DANIEL L., CARTER, GLENN S., TODD, ROBERT E. & COLE, SYLVIA T. 2011 Internal tidal beams and mixing near monterey bay. *Journal of Geophysical Research: Oceans* **116** (C3).

KARIMI, HUSSAIN H. 2015 Parametric subharmonic instability of internal gravity wave beams. PhD thesis, Massachusetts Institute of Technology.

KARIMI, HUSSAIN H. & AKYLAS, T. R. 2014 Parametric subharmonic instability of internal waves: locally confined beams versus monochromatic wavetrains. *Journal of Fluid Mechanics* **757**, 381–402.

KATAOKA, T. & AKYLAS, T. R. 2013 Stability of internal gravity wave beams to three-dimensional modulations. *Journal of Fluid Mechanics* **736**, 67–90.

KATAOKA, T. & AKYLAS, T. R. 2015 On three-dimensional internal gravity wave beams and induced large-scale mean flows. *Journal of Fluid Mechanics* **769**, 621–634.

KATAOKA, T. & AKYLAS, T. R. 2016 Three-dimensional instability of internal gravity wave beams. In *Proceedings of the VIII International Symposium on Stratified Flows, San Diego, 29 August-1 September 2016* (ed. University of California at San Diego).

KING, BENJAMIN, ZHANG, H. P. & SWINNEY, HARRY L. 2009 Tidal flow over three-dimensional topography in a stratified fluid. *Physics of Fluids* **21** (11), –.

LELONG, M. PASCALE & RILEY, JAMES J. 1991 Internal wave—vortical mode interactions in strongly stratified flows. *Journal of Fluid Mechanics* **232**, 1–19.

LIGHTHILL, M. J. 1978 *Waves in Fluids*. Cambridge University Press.

MACKINNON, J. A., ALFORD, M. H., SUN, OLIVER, PINKEL, ROB, ZHAO, ZHONGXIANG & KLYMAK, JODY 2013 Parametric subharmonic instability of the internal tide at 29°n. *Journal of Physical Oceanography* **43** (1), 17–28.

MAURER, P., JOUBAUD, S. & ODIER, P. 2016 Generation and stability of inertia–gravity waves. *Journal of Fluid Mechanics* **808**, 539–561.

MCINTYRE, M. E. & NORTON, W. A. 1990 Dissipative wave-mean interactions and the transport of vorticity or potential vorticity. *Journal of Fluid Mechanics* **212**, 403–435.

MERCIER, MATTHIEU J., MARTINAND, DENIS, MATHUR, MANIKANDAN, GOSTIAUX, LOUIS, PEACOCK, THOMAS & DAUXOIS, THIERRY 2010 New wave generation. *Journal of Fluid Mechanics* **657**, 308–334.

MOWBRAY, D. E. & RARITY, B. S. H. 1967 A theoretical and experimental investigation of the phase configuration of internal waves of small amplitude in a density stratified liquid. *Journal of Fluid Mechanics* **28**, 1–16.

MÜLLER, PETER 1995 Ertel's potential vorticity theorem in physical oceanography. *Reviews of Geophysics* **33** (1), 67–97.

PLUMB, R. A. 1977 The interaction of two internal waves with the mean flow: Implications for the theory of the quasi-biennial oscillation. *Journal of the Atmospheric Sciences* **34** (12), 1847–1858.

RILEY, N 2001 Steady streaming. *Annual Review of Fluid Mechanics* **33** (1), 43–65.

SHRIRA, V. I. 1981 On the propagation of a three-dimensional packet of weakly non-linear internal gravity waves. *International Journal of Non-Linear Mechanics* **16** (2), 129–138.

STAQUET, C. & SOMMERIA, J. 2002 Internal gravity waves: from instabilities to turbulence. *Annual Review of Fluid Mechanics* **34** (1), 559–593.

SUTHERLAND, BRUCE R. 2001 Finite-amplitude internal wavepacket dispersion and breaking. *Journal of Fluid Mechanics* **429**, 343–380.

SUTHERLAND, BRUCE R. 2010 *Internal Gravity Waves*. Cambridge University Press.

SUTHERLAND, BRUCE R. 2013 The wave instability pathway to turbulence. *Journal of Fluid Mechanics* **724**, 1–4.

TABAEI, ALI & AKYLAS, T. R. 2003 Nonlinear internal gravity wave beams. *Journal of Fluid Mechanics* **482**, 141–161.

TABAEI, ALI & AKYLAS, T. R. 2007 Resonant long–short wave interactions in an unbounded rotating stratified fluid. *Studies in Applied Mathematics* **119** (3), 271–296.

TALLEY, LYNNE 2011 *Descriptive Oceanography*, 6th edn. Elsevier Ltd.

WUNSCH, CARL & FERRARI, RAFFAELE 2004 Vertical mixing, energy, and the general circulation of the oceans. *Annual Review of Fluid Mechanics* **36** (1), 281–314.

YUEN, H C & LAKE, B M 1980 Instabilities of waves on deep water. *Annual Review of Fluid Mechanics* **12** (1), 303–334.